2015

# Enhanced Microwave Hyperthermia using Nanoparticles

Maryory Urdaneta
*University of Central Florida*

# ENHANCED MICROWAVE HYPERTHERMIA USING NANOPARTICLES

by

MARYORY URDANETA
M.S. University of Central Florida, 2012

A dissertation submitted in partial fulfillment of the requirements
for the degree of Doctor of Philosophy
in the Department of Electrical Engineering and Computer Science
in the College of Engineering and Computer Science
at the University of Central Florida
Orlando, Florida

Spring Term
2015

Major Professor: Parveen Wahid

# ABSTRACT

In this dissertation a study of enhanced hyperthermia for cancer treatment through the use of magnetic nanoparticles is presented. Hyperthermia has been in use for many years, as a potential alternative method in cancer treatment, and high frequency microwave radiation has been used successfully to raise the tumor temperature to around 42°C in superficial tumors without causing damage to surrounding healthy tissues. Magnetic fluid hyperthermia involves the use of magnetic nanoparticles injected into the tumor before exposure to microwave radiation. The magnetic energy in the nanoparticles is converted into heat allowing for a more rapid rise of temperature in the tumor to the desired level. In addition, the nanoparticles allow the electromagnetic absorption to be focused in the tumor and can be used to treat deep tumors in organs, such as the liver. Iron oxide magnetic nanoparticles were considered for this study as they are non-toxic and bio-compatible. For the case of breast cancer, the values for the temperature and specific absorption rate (SAR) in the tumor and in the healthy tissue were obtained through simulations and validated by measurement done on phantom models. Various characteristics of the nanoparticles such as radius, magnetic susceptibility and concentration were considered. In order to take the effect of the blood flow, which causes cooling and helps maintain the body temperature, various blood perfusion rates for a tumor in the liver were studied. A human male model in SEMCAD X, in which blood flow can be adjusted, was used for simulations. The tumor was injected with the nanoparticles and the change in temperature upon exposure to electromagnetic radiation was observed. The simulated results were compared with measured results on a liver phantom model in which saline solution was used to model blood flow. There was good agreement between the measured and simulated results.

# ACKNOWLEDGMENTS

I would like to thank my advisor Dr. Wahid for all her support, guidance and patient during my studies at UCF. Thanks for giving me the opportunity to work with you. I could not ask for more from you. I also appreciate the helpful teachings and guidance of my dissertation committee members: Prof. Xun Gong, Prof. Kalpathy Sundaram, Prof. Samuel Richie and Prof. Suryanarayana Challapalli.

I also thankfully acknowledge SEMCAD X for providing the simulation tools to accomplish this research.

I am thankful to the Fulbright Scholarship program for their support at the beginning of my career. Without their support I would not have started this amazing adventure.

Thanks to all of my course professors. I learned so much from all of you that will surely benefit me for the rest of my life.

I am eternally grateful to my family who has supported me throughout my life, even from a distance. I thank my mother Marisela for her enduring love, support and patience. I would not have completed this step in my career without you in my corner.

I am truly thankful to all members of the ARMI lab at UCF who generously offered their time to help anytime I needed it.

Thanks to my alma mater Universidad del Zulia for their support me throughout all these years.

# TABLE OF CONTENTS

LIST OF FIGURES ..... vi
LIST OF TABLES ..... viii
CHAPTER 1: INTRODUCTION ..... 1
1.1. Overview of Medical Applications of High Frequency Radiation ..... 1
1.1.1. Microwave Imaging ..... 1
1.1.2. Thermal Therapy ..... 2
1.2. Motivation for the Research ..... 4
1.3. Dissertation Outline ..... 5
CHAPTER 2: BIOLOGICAL AND PHYSICAL ASPECTS OF HYPERTHERMIA ..... 7
2.1. RF/Microwave Propagation in Biological Tissues ..... 7
2.2. Electromagnetic Waves Propagating in Biological Tissues ..... 7
2.3. Hyperthermia ..... 11
2.4. Hyperthermia Applicators ..... 12
2.4.1. Inductive Heating ..... 13
2.4.2. Capacitive Heating ..... 13
2.4.3. Radiation Heating ..... 14
2.4.4. Interstitial Applicators ..... 14
CHAPTER 3: HEAT TRANSFER IN HYPERTHERMIA ..... 15
3.1. Introduction ..... 15
3.2. Penne's Bioheat Equation ..... 15
3.3. Specific Absorption Rate (SAR) ..... 16
CHAPTER 4: MAGNETIC FLUID HYPERTHERMIA ..... 19
4.1. Introduction ..... 19
4.2. Nanoparticle Targeting ..... 20
4.3. Heat Generation of Nanoparticles ..... 20
4.3.1. Hysteresis ..... 21
4.3.2. Relaxation ..... 22
CHAPTER 5: MICROWAVE MAGNETIC FLUID HYPERTHERMIA MODELING ..... 29

5.1. Introduction ..... 29
5.2. Magnetic Fluid Hyperthermia Design Considerations ..... 29
5.3. Heat Generation ..... 30
5.4. Simulation ..... 31
5.5. Temperature Measurements using SEMCAD X ..... 32
5.6. Effect of Nanoparticle Characteristics in the Transient Temperature in the Tumor ..... 35
5.6.1. Nanoparticle Size ..... 36
5.6.2. Nanoparticle Susceptibility ..... 38
5.6.3. Effect of Nanoparticle Concentration on the Heating Behavior ..... 38
5.6.4. Optimization of Nanoparticle Concentration ..... 39
5.7. Experimental Results ..... 41
5.7.1. Solid Phantom ..... 41
5.7.2. Measurement Setup ..... 43
5.7.3. Temperature Measurements ..... 43
CHAPTER 6: MAGNETIC FLUID HYPERTHERMIA INCORPORATING BLOOD FLOW 46
6.1. Introduction ..... 46
6.2. Blood Perfusion in Humans ..... 46
6.3. Magnetic Fluid Hyperthermia Design Incorporating the Blood Perfusion ..... 48
6.4. Simulated Transient Temperature ..... 50
6.5. Experimental Results using a Simplified Phantom ..... 56
6.6. Measured Temperatures ..... 59
6.7. Use of Magnetic Fluid Hyperthermia in Human Tissues ..... 62
CHAPTER 7: CONCLUSIONS ..... 63
REFERENCES ..... 65

# LIST OF FIGURES

Figure 1. Microwave imaging of breast tissue ..... 2
Figure 2. Electric field propagation in biological tissues ..... 8
Figure 3. Relative absorbed power in fat and muscle as a distance function at 2.45 GHz ..... 9
Figure 4. a) Large particles hysteresis, b) Small particles hysteresis and c) Smaller particles hysteresis ..... 21
Figure 5. Real and imaginary components of the susceptibility vs. Frequency ..... 25
Figure 6. Hyperthermia system configuration ..... 29
Figure 7. Breast tissue model in SEMCAD X ..... 32
Figure 8. Tempertaure distribution during hyperthermia without nanoparticles ..... 33
Figure 9. Tempertaure distribution during hyperthermia with nanoparticles ..... 34
Figure 10. Time temperature increase in the tissue as function of distance from the applicator .. 35
Figure 11. Transient temperature in the tumor for different nanoparticles sizes ..... 36
Figure 12. Néel relaxation time $\tau N$ as a function of radius of the nanoparticle ..... 37
Figure 13. Transient temperature in the tumor for different nanoparticles susceptibilities ..... 38
Figure 14. Transient temperature in the tumor with different nanoparticles concentrations ..... 39
Figure 15. Solid phantom simulating the human breast tissue ..... 42
Figure 16. Ferrofluid conatining the nanoparticles and tumor phantom ..... 42
Figure 17. Measurement setup ..... 43
Figure 18. Temperature in phantom without nanoparticles ..... 44
Figure 19. Temperature in phantom with nanoparticles ..... 45
Figure 20. Human model in SEMCAD X ..... 49
Figure 21. Transient temperature in the l.iver model – Blood perfusion rate 100% ..... 51
Figure 22. Transient temperature in the l.iver model – Blood perfusion rate 75% ..... 51
Figure 23. Transient temperature in the liver model – Blood perfusion rate 50% ..... 52
Figure 24. Transient temperature in the l.iver model – Blood perfusion rate 25% ..... 52
Figure 25. Transient temperature in the l.iver model – Blood perfusion rate 5% ..... 53
Figure 26. Temperature comparison in the tumor and healthy tissue ..... 54

Figure 27. SAR comparison in the tumor and healthy tissue ..... 54
Figure 28. Temperature increase in the tumor as a function of nanoparticle concentration..... 55
Figure 29. Simplified liver model..... 56
Figure 30. Liver phantom measurement setup – Side view..... 58
Figure 31. Liver phantom model – Top view ..... 58
Figure 32. Temperature measured in healthy and tumor tissues in the model 1 ..... 59
Figure 33. Temperature measured in healthy and tumor tissues in the model 2 ..... 60
Figure 34. Temperature measured in healthy and tumor tissues in the model 3 ..... 60
Figure 35. Temperature measured in healthy and tumor tissues in the model 4 ..... 61
Figure 36. Temperature measured in healthy and tumor tissues in the model 5 ..... 61

# LIST OF TABLES

Table 1. Dielectric properties of human tissues at different frequencies ..... 10

Table 2. Basic restrictions for time varying electric and magnetic fields for frequencies up to 10 GHz. ..... 17

Table 3. Electrical properties of human tissues ..... 30

Table 4. Thermal properties of human and tumor tissues ..... 31

Table 5. Blood perfusion in human tissues ..... 47

Table 6. Models with different blood perfusion rates ..... 50

# CHAPTER 1: INTRODUCTION

## 1.1.Overview of Medical Applications of High Frequency Radiation

The radio frequency spectrum spans the range of 3 kHz to several hundred GHz. The microwave region, which is from 1 GHz to around 30 GHz, is the portion of the electromagnetic spectrum that is nonionizing, that is, this radiation does not have enough energy to ionize atoms or molecules. Thus, this nonionizing radiation can be very useful in biomedical applications [1, 2]. Transmission, absorption and reflection of the electromagnetic energy will depend on the body size, tissue properties, and the frequency of the radiation [3].

Non-ionizing electromagnetic fields, in the RF/MW range, have been used in various medical treatments. The most common applications are diagnostic imaging and therapeutic applications.

### 1.1.1. Microwave Imaging

Currently available diagnostic screening systems for cancer include X-ray computed tomography (CT) and mammography. They are effective at detecting early signs of tumors, however, they are far from perfect, subjecting patients to ionizing radiation. Mammography can inflict discomfort on women who are undergoing screening because of the compression of the breast that is required to produce diagnostically useful images.

A better, cheaper, and safer way to detect breast cancer is possible with microwaves. Microwave imaging relies upon the known differences in the dielectric properties of cancerous tissue and normal tissue, that is, their ability to conduct electricity or sustain an electric field. In

the technique, the tissue is irradiated using an array of antennas surrounding the tissue. An example of the set up for use with a breast tissue is shown in Figure 1. Each antenna illuminates the tissue individually with a very low power microwave signal, with approximately one one-thousandth the power of a cell phone, while the other antennas receive the signals transmitted through the tissue. This process is repeated for each antenna, providing data that can be used to produce a 3-D representation of the tissue, including the location of both the normal and the cancerous tissue.

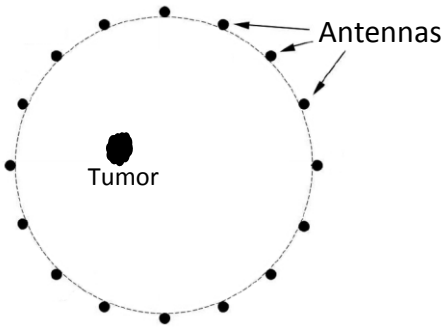


Figure 1. Microwave imaging of breast tissue

### 1.1.2. Thermal Therapy

In thermal therapy, the body tissue is exposed to high temperatures to damage and kill cancer cells or to make cancer cells more sensitive to the effects of radiation and certain anticancer drugs.

Absorption of RF/MW radiation which results in the heating of the body tissues depends on several factors. These include wavelength of the radiation and the tissue properties.

Frequencies greater than 10,000 MHz (10 GHz) are absorbed mostly in the outer skin. Frequencies between 10,000 MHz and 2500 MHz penetrate more deeply, approximately 3 mm to 2 cm into the tissue. Frequencies of 2500 MHz to 1300 MHz penetrate deep enough to cause damage to internal organs by overheating of the tissue [4].

There are a growing number of clinical applications of thermal therapy that benefit patients with a variety of diseases, such as hyperthermia and thermal ablation.

Hyperthermia: In the late 1950s, it was determined that raising the tumor to temperatures of 42 - 45 °C made them more sensitive to radiation/chemotherapy. This technique has been proven effective over the past 20 years through clinical trials. The combination of hyperthermia with radiation therapy has been shown to and improve treatment efficacy, tumor response and duration of local tumor control. Hyperthermia has been proven successful in the treatment of recurrent chest wall breast cancer, melanoma, locally advanced head and neck cancer, and several other cancers. Today, in some countries such as The Netherlands and Germany, hyperthermia is part of standard cancer care.

Thermal ablation: In this treatment the tissue is destroyed by localized heating or freezing. Various energy sources including laser, ultrasound and microwaves are found to be minimally invasive, and potentially useful for this therapy.

Today, according the Society for Thermal Medicine, about 100,000 patients with cancers of the liver, lung, kidney and bone are annually treated worldwide using thermal therapy, as it provides local tumor control with minimal side effects. About a dozen FDA approved devices are available, with novel devices in the pipeline [5]. In addition, the combination of thermal

ablation with chemo- or radiation therapy, and immunotherapy, is being pursued in clinical trials [6, 7].

### 1.2. Motivation for the Research

Cancer remains one of the leading causes of death in the world. New methods for treatment of cancer that have been implemented have been successful, but the results are still limited. The use of hyperthermia along with conventional cancer treatment such as chemotherapy and radiation has been successful in many cancer treatments [6, 7]. In this approach, the cancerous tumors are heated to a temperature between 40 and 45°C for a specific period of time which renders tumor cells more sensitive to radiation and chemotherapy. The increase in temperature stimulates blood flow in the tumor, increases oxygenation and hence makes the treatment more effective. High temperatures can kill cancer cells, but they also can injure or kill normal cells and tissues. Temperatures above 42°C can cause burns and blisters in healthy tissue. Consequentially, during hyperthermia treatment, the temperature in the tumor and healthy tissue has to be closely monitored.

In hyperthermia, suitable applicators (antennas) are used to provide energy to penetrate the body tissues. A majority of the applicators provide good energy deposition in superficial tumors [8, 9]. For treating deep seated tumors, the frequency of the applicators is lower, and typically and array of applicators is used as a single applicator may not provide the necessary energy. With the hyperthermia systems developed for regional hyperthermia of deep seated tumors, selective heating of those regions is still very difficult. Moreover, in almost all clinical trials patients experienced local pain and discomfort and the temperature in healthy tissues was also high [10].

The main concern in deep hyperthermia is the power deposition in tumors and the temperature monitoring during treatment. The current procedures have a limitation on the body target sites that are too difficult to treat. There is a large need for alternative effective options in hyperthermia for providing deep seated power deposition various regions of the body, without affecting healthy surrounding tissues and organs.

Hence, in this research we investigate an enhanced hyperthermia treatment through the use of magnetic nanoparticles.

### 1.3. Dissertation Outline

This dissertation consists of 7 major sections. The first chapter is an overview of the use of high frequency in medicine. It introduces the hyperthermia cancer treatment and the motivation for this research.

Chapter 2 covers the biological and physical aspects of hyperthermia. The biological aspects of hyperthermia refers to the electromagnetic propagation in biological tissues and the physical aspects cover the applicators used in hyperthermia treatments.

Chapter 3 explains in detail the heat transfer in microwave hyperthermia using the bioheat equation and study the specific absorption rate.

Chapter 4 details the use of magnetic nanoparticles in hyperthermia. The nanoparticle targeting mechanisms and the heat generated by using nanoparticles during hyperthermia treatment are presented.

Chapter 5 focuses on a primary study of microwave hyperthermia in breast cancer treatment using magnetic nanoparticles. The results of simulation and measurement are included in this chapter.

Chapter 6 presents results for an enhanced hyperthermia treatment for liver cancer with realistic human models incorporating the blood perfusion rate. Here, the results of simulations and measurement are presented.

Conclusions of this research are presented in Chapter 7.

# CHAPTER 2: BIOLOGICAL AND PHYSICAL ASPECTS OF HYPERTHERMIA

## 2.1. RF/Microwave Propagation in Biological Tissues

The interaction of the high frequency fields with the biological tissues is determined to a large extent by the characteristics of the tissue permittivity ε, permeability μ and conductivity σ. Biological tissues are non-magnetic and hence the permeability μ does not play a major role. There are several sources in the literature [11, 12] where the ε, μ and σ values for various tissues such as muscles, bone, blood, liver, kidney, etc., at various frequencies are provided. Table 1 shows the dielectric properties of human tissues at 3 different frequencies 915 MHz, 2.45 GHz and 10 GHz. Heat absorption will be greatest in tissues that have high water content, such as muscle, with less heat absorption taking place in bone and fat [12].

## 2.2. Electromagnetic Waves Propagating in Biological Tissues

When the biological tissues are exposed to RF/Microwave radiation, the characteristics of the tissues will determine the amount of energy reflected by or absorbed in the tissue.

Consider a tissue with an incident linearly polarized EM wave propagating along z direction, as shown in Figure 2, with its E field polarized along x direction and H field polarized along y direction. $E_i$ is the incident electric field, $E_t$ is the transmitted electric field and $E_r$ is the reflected electric field.

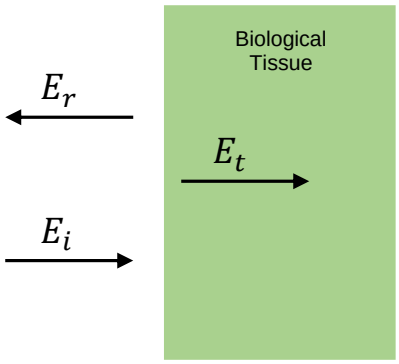

Figure 2. Electric field propagation in biological tissues

The field inside the tissue can be written as:

$$E_t = E_0 e^{-\alpha z} \quad (1)$$

were $E_0$ is the amplitude of the incident wave and α is the attenuation constant of the medium.

The skin depth $\delta$, is the distance at which the field reduces to 37% of its value at the interface, is equals to $1/\alpha$.

The frequency of the radiation and the dielectric properties of the tissue determine the penetration of energy in the human tissues. Figure 3 shows the effect of the skin depth on the power absorbed in fat and muscle tissue at 2.45 GHz. The skin depth for fat is 0.117 m and for muscle 0.022 m, calculated using values in Table 1. At this frequency, the penetration is deeper in the fat tissue showing a higher level of absorbed power.

The skin effect implies that, when using microwaves for a medical application, the higher the frequency, the smaller the penetration, which may lower the efficiency of the application. Hence, the choice of frequency is important. It also implies that if a human being, for instance, is submitted to a microwave field, the internal organs are more protected at higher than at lower frequencies.

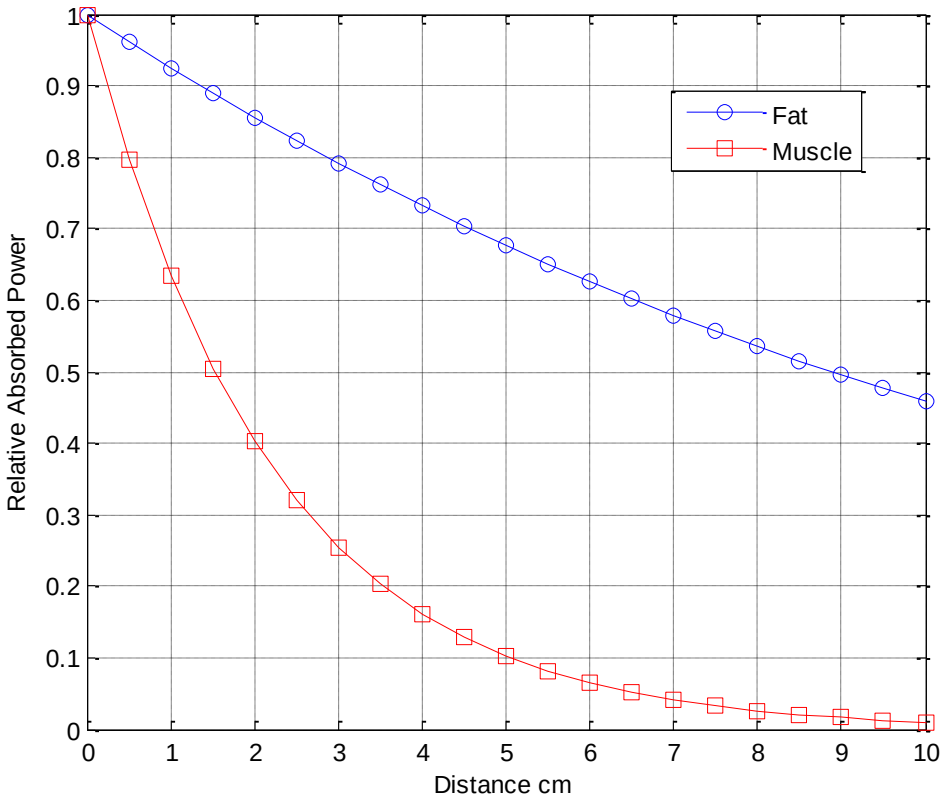


Figure 3. Relative absorbed power in fat and muscle as a distance function at 2.45 GHz

Table 1. Dielectric properties of human tissues at different frequencies

| | 915 MHz | | | 2.45 GHz | | |
|---|---|---|---|---|---|---|
| **Tissue Name** | **Conductivity [S/m]** | **Relative permittivity** | **Loss tangent** | **Conductivity [S/m]** | **Relative permittivity** | **Loss tangent** |
| Bladder | 0.38506 | 18.923 | 0.39976 | 0.68532 | 18.001 | 0.27933 |
| Blood | 1.5445 | 61.314 | 0.49487 | 2.5448 | 58.264 | 0.32046 |
| Blood Vessel | 0.70087 | 44.741 | 0.30774 | 1.4353 | 42.531 | 0.2476 |
| Bone Cancello | 0.34353 | 20.756 | 0.32515 | 0.80517 | 18.548 | 0.31849 |
| Bone Cortical | 0.14512 | 12.44 | 0.22919 | 0.39431 | 11.381 | 0.2542 |
| Bone Marrow | 0.040588 | 5.5014 | 0.14494 | 0.095037 | 5.2969 | 0.13164 |
| Breast Fat | 0.049523 | 5.4219 | 0.17944 | 0.13704 | 5.1467 | 0.19535 |
| Cartilage | 0.7892 | 42.6 | 0.36394 | 1.7559 | 38.77 | 0.33228 |
| Colon | 1.087 | 57.867 | 0.36901 | 2.0383 | 53.879 | 0.27757 |
| Cornea | 1.4008 | 55.172 | 0.49878 | 2.2954 | 51.615 | 0.32629 |
| Fat | 0.051402 | 5.4596 | 0.18496 | 0.10452 | 5.2801 | 0.14524 |
| GallBladder | 1.2614 | 59.118 | 0.41918 | 2.059 | 57.634 | 0.26212 |
| Heart | 1.2378 | 59.796 | 0.40668 | 2.2561 | 54.814 | 0.30199 |
| Kidney | 1.4007 | 58.556 | 0.46991 | 2.4295 | 52.742 | 0.33797 |
| Liver | 0.86121 | 46.764 | 0.36179 | 1.6864 | 43.035 | 0.28751 |
| Muscle | 0.94809 | 54.997 | 0.33866 | 1.7388 | 52.729 | 0.24194 |
| Nerve | 0.57759 | 32.486 | 0.34929 | 1.0886 | 30.145 | 0.26494 |
| Prostate | 1.2159 | 60.506 | 0.39477 | 2.1676 | 57.551 | 0.27633 |
| Retina | 1.1725 | 55.23 | 0.41706 | 2.0332 | 52.628 | 0.28345 |
| Skin | 0.87169 | 41.329 | 0.41435 | 1.464 | 38.007 | 0.28262 |
| Small Intestin | 2.173 | 59.389 | 0.71881 | 3.1731 | 54.425 | 0.42777 |
| Spinal Cord | 0.57759 | 32.486 | 0.34929 | 1.0886 | 30.145 | 0.26494 |
| Stomach | 1.1932 | 65.02 | 0.36053 | 2.2105 | 62.158 | 0.36053 |
| Tooth | 0.14512 | 12.44 | 0.22919 | 0.39431 | 11.381 | 0.2542 |

The amount of power deposition in the body is be expressed through the specific absorption rate (SAR), measured in watts per kilogram of mass tissue and is a simple and useful value for quantifying the interactions of RF/microwave radiation with living systems. The SAR is defined as the ratio of the total power absorbed in the exposed body to the mass in which it is absorbed, which is not necessarily that of the total body:

$$SAR = \frac{\sigma E^2}{\rho} \quad (2)$$

where E is the root mean square electric field [V/m], σ is the conductivity [S/m], and ρ is the mass density of the tissue [kg/m$^3$].

### 2.3. Hyperthermia

The normal temperature in a human body is 37°C. Hyperthermia refers to increase in the normal temperature in the human body. In hyperthermia treatment, cancerous cells temperatures are elevated to the range between 42 - 45°C, so as to destroy them. This treatment can be done without substantial damage to healthy tissues and with minimal side effects. Hyperthermia cancer treatment is been used nowadays in combination with radiotherapy and chemotherapy.

Hyperthermia can be used to treat specific tumor locations or for the entire body. In local hyperthermia, used to increase the temperature in a specific area that contains a tumor, the heat generation can be achieved by external applicators to treat tumors near the skin's surface or with probes to reach deep-seated cancerous tissues. Regional hyperthermia is used for larger or

multiple tumor locations or to treat cancers that have spread to several regions. Here, a larger part of the body is heated to destroy the cancerous cells [13, 14]. This treatment is also usually combined with chemotherapy or radiation therapy.

In hyperthermia treatment, the high frequency electromagnetic energy is applied to the tissue using either external or internal applicators depending on the tumor location. Internal applicators use a needle or probe to release the energy directly into the tumor, and external applicators radiate the tissue from outside.

Healthy tissues can also absorb electromagnetic energy and get heated leading to burns, blisters, and discomfort. Thus, it is critical to monitor temperatures in healthy tissues during hyperthermia treatment.

### 2.4. Hyperthermia Applicators

Electromagnetic hyperthermia used before the 1950s was not well developed and mainly empirical [15, 16]. After 1950, hyperthermia as a separate treatment modality started [17]. Research work was focused on the development of quasi-static or radiative techniques using electromagnetic energy. Initially, these devices operated only at the ISM (Industry Science and Medicine) frequencies, and typically had a single power source, one applicator and limited treatment area. Electric and magnetic field were used to deliver the electromagnetic energy to the patient through the air. Over the years, various applicators were developed to provide better tissue deposition and maintain heterogeneous skin cooling. In addition, several advanced computer aided design allowed the design of efficient applicators [18-22].

### 2.4.1. Inductive Heating

For inductive heating, an inductive concentric coil is placed around the patient avoiding contact between the patient and the applicator. The electromagnetic energy is transferred through magnetic fields. It was found that one main disadvantage of these devices is that the power deposition at the center of the target tissue is very low [23].

In order to solve this problem, a helical coil applicator with a coaxial pair magnetic system was developed [24]. This device creates homogeneous energy deposition in the patient by moving the applicator around its longitudinal axis. It operates at its resonance frequency and creates eddy currents by the inductive field component. However, this device had limited spatial control of the energy deposition and the blood perfusion played an important role in the tumor heating.

### 2.4.2. Capacitive Heating

Here, the electric field is used to transfer the electromagnetic energy to the tissue, with one electrode placed below and one above the patient [25]. The energy deposition depends on the sizes of electrodes and the electric field. It is seen that there is a high power deposition in the subcutaneous fatty tissue. The disadvantages of this devices is that the energy distribution will depend only on the electrodes position and size and hence the treatment needs to be stopped to make any change in electrodes. The blood perfusion plays and important role in the tumor heating [25].

### 2.4.3. Radiation Heating

Cylindrical waveguides and dipole antennas are used as radiating devices for radiation heating [26]. The main disadvantage with these applicators is that the volume treated is very small and the antennas used have low directivity. The radiating elements are divided into devices for use in superficial hyperthermia and for deep hyperthermia, based on the frequency and tumor location.

When the tumors are superficial, less number of applicators are needed. Multi-elements applicators are used to obtain a high heterogeneity of SAR distribution [27-30].

### 2.4.4. Interstitial Applicators

The electromagnetic energy can also be delivered to the diseased tissue through an invasive process where antennas (needles) are inserted into the tumor. These are placed inside the patient using imaging guidance, such as CT (computed tomography) or ultrasound. These applicators can also be used during an open surgical procedure to target and ablate the diseased soft-tissue [31].

Due to the invasive nature of this technique, these applicators can cause discomfort and complications prior to, during and after each treatment.

# CHAPTER 3: HEAT TRANSFER IN HYPERTHERMIA

## 3.1. Introduction

For hyperthermia, the temperature increase in the tissues during electromagnetic heating needs to be determined accurately. Heat transfer analysis often needs to simultaneously deal with transient and spatial heating inside biological bodies. The Penne's bioheat transfer equation, which describes the exchange magnitude of heat transfer between tissue and blood, is widely used to solve the temperature distribution for thermal therapy [32-33]. The Penne's bioheat transfer equation is based on the assumption that all heat transfer between the tissue and the blood occurs in the capillaries, and neglects the local effects where "thermally significant" blood vessels do not appear in the temperature field. For localized hyperthermia, Ocheltree and Frizzell [34 -35] demonstrated the analytical formulations for both transient and steady state of three tumor models via the Penne's bioheat transfer equation.

## 3.2. Penne's Bioheat Equation

For the transient problem, the Penne's bioheat transfer equation is given as

$$\rho_t c_t \frac{\partial T}{\partial t} = k \frac{\partial^2 T}{\partial x^2} - \omega_b \rho_b c_b (T - T_a) + Q_{met} + Q_{ext} \qquad (3)$$

where $\rho_t$ is the tissue density, $c_t$ is the specific heat of tissue, $T$ is the tissue temperature, $\omega_b$ is the blood perfusion rate, $\rho_b$ is the blood density, $c_b$ is the specific heat of blood, $T_a$ is the tissue

temperature, $k$ is the thermal conductivity of tissue, $Q_{met}$ is the heat coming from metabolism, $Q_{ext}$is the absorbed power due to an external source and can be written as:

$$Q_{ext} = \frac{1}{2}\sigma_t |E|^2 \quad (4)$$

where $\sigma_t$ is the electrical conductivity of the tissue and E is the electric field generated by the EM applicator. By analyzing (4), it is evident that only the E field is taken into account to obtain the temperature increase in tissues and tumors. Although the EM applicator generates E and H fields, the effect of the H field is neglected because biological tissues are nonmagnetic.

### 3.3. Specific Absorption Rate (SAR)

The specific absorption rate (SAR) is a measure of the energy absorbed by the tissue due to electromagnetic radiation and is related to the increase in temperature in the tissue. The SAR is the ratio of the total power absorbed in the exposed body to the mass in which it is absorbed, as explained in Section 2.2. The amount of energy absorbed by the tissue depends on several factors including frequency, dielectric property of the tissue, irradiating time exposure, intensity of electromagnetic radiation, and water content of the tissue.

As exposure to high frequency electromagnetic radiation can cause damage to tissues, there are strict safety guidelines for exposure that are set by the Federal Communications Commission FCC [36, 37].

In sensitive organs, small temperature increases can produce severe physiological effects. An increase of approximately 1–5°C in human body temperature can cause numerous

malformations, temporary infertility in males, brain lesions, and blood chemistry changes. Even a small temperature increase in human body (approximately 1°C) can lead to altered production of hormones and suppressed immune response [36].

At high frequencies human tissues with finite electric conductivity are generally lossy mediums and are usually neither good dielectric materials nor good conductors and as electromagnetic waves propagate through the human tissues, the energy of EM waves is absorbed by the tissues.

The basic restrictions for whole body average SAR, and localized SAR for frequencies between 1 Hz and 10 GHz, according to IEEE Standards, are presented in Table 2 [36]:

Table 2. Basic restrictions for time varying electric and magnetic fields for frequencies up to 10 GHz.

| Frequency Range | Localized SAR (head and trunk) ($W\ kg^{-1}$) | Localized SAR (limbs) ($W\ kg^{-1}$) |
|---|---|---|
| Up to 100 kHz | - | - |
| 100 kHz – 10 MHz | 2 | 4 |
| 10 MHz – 10 GHz | 2 | 4 |

In the low-frequency range, there are currently few data relating transient currents to health effects. The ICNIRP therefore recommends that the restrictions on current densities induced by transient or very short-term peak fields be regarded as instantaneous values which should not be time-averaged [36].

The SAR values in the tissue which are an indicator of energy absorption, can be related to the temperature rise in the tissue. The absorbed energy is converted to heat that results in the temperature increase. The SAR can also be expressed in terms of the temperature gradient ($\Delta T$) induced in the system:

$$SAR = c\frac{\Delta T}{\Delta t} \tag{5}$$

where $c$ is the specific heat of the tissue and $\Delta t$ is the treatment time. This definition relates the temperature changes in the tissue to the SAR values in the tissue.

# CHAPTER 4: MAGNETIC FLUID HYPERTHERMIA

## 4.1. Introduction

Nanoparticles are microscopic particles with dimensions of less than 100 nm. They possess a wide variety of potential applications and are now used for medical diagnosis and for treatment. Fluorescent semiconductor nanoparticles, known as quantum dots, are used for imaging of biological entities [38] and superparamagnetic nanoparticles are used as contrast agents for magnetic resonance imaging (MRI) to help diagnose various diseases [39].

The multifunctional characteristic of nanoparticles makes them great candidates for targeted drug delivery and cancer treatment, and they are currently in use as anti-cancer drug and gene carriers for controlling cancer [40].

For cancer therapy, the nanoparticle distribution within the body depends on various parameters such as their relatively small size resulting in longer circulation times and their ability to take advantage of tumor characteristics. For example, nanoparticles less than 20 nm in size are able to pass through blood vessel walls and such small particle size allows for intravenous injection as well as intramuscular and subcutaneous applications. The small size of the nanoparticles minimizes the irritant reactions at the injection site as compared to conventional cancer treatments. Furthermore, nanoparticle size allows for interactions with biomolecules on the cell surfaces and within the cells without altering the behavior and biochemical properties of those molecules [41].

Nanoparticles can be formulated for specific uptake within the body and for a specific response by the body to cancer treatment. Nanoparticles can be formulated from a variety of

materials so as to carry substances in a controlled and targeted manner. Synthetic polymers, which are bio-degradable, are used to prepare the nanoparticles for drug delivery. In transportation, this prevents degradation of the carried load and also protects transported substances from contact with healthy tissues, hence reducing side effects and increasing the relative amount of the load reaching the diseased tissue.

### 4.2. Nanoparticle Targeting

In treatments using nanoparticles, the goal is to have them reach the desired tumor sites, after administration, with minimal loss to their volume and activity in blood circulation and to attach to tumor cells without harmful effects to healthy tissue. This may be achieved using two strategies: passive and active targeting of drugs.

Passive drugs targeting consists in the transport of nanoparticles through tumor capillaries by convection or passive diffusion [42]. Tumor vessels are highly disorganized and dilated with a high number of pores, resulting in enlarged gap junctions between endothelial cells and compromised lymphatic drainage. In this case, nanoparticles may be released in the extracellular matrix and then diffused through the tumor tissue.

In active targeting, targeting ligands are attached at the surface of the nanoparticle for binding to appropriate receptors expressed at the tumor site. The ligand is chosen to bind to a receptor of specific tumor cells and not expressed by normal cells [42].

### 4.3. Heat Generation of Nanoparticles

When nanoparticles are exposed to an electromagnetic field, they transform the energy of the electromagnetic field into heat by different mechanisms. This transformation depends on the

frequency of the external field and on the characteristics of the particles such as their size and other characteristics [43 – 45].

### 4.3.1. Hysteresis

Hysteresis exhibited by magnetic nanoparticles varies depending on the particle size. This is shown in Figure.4. Large particles (on the order of microns or more) exhibit a narrow hysteresis loop because it takes little magnetic field energy to make the domain walls move compared to the energy required to rotate the magnetic moment of the particle. Small particles exhibit a broad hysteresis loop. In smaller sizes (on the order of tens of nanometers or less) superparamagnetism is observed. These particles have no hysteresis loop because the magnetic moment of the particle as a whole is oscillating in response to the thermal energy at room temperature. Therefore, superparamagnetic nanoparticles exhibit heat dissipation when exposed to an electromagnetic field due to the magnetic relaxation loss [46].

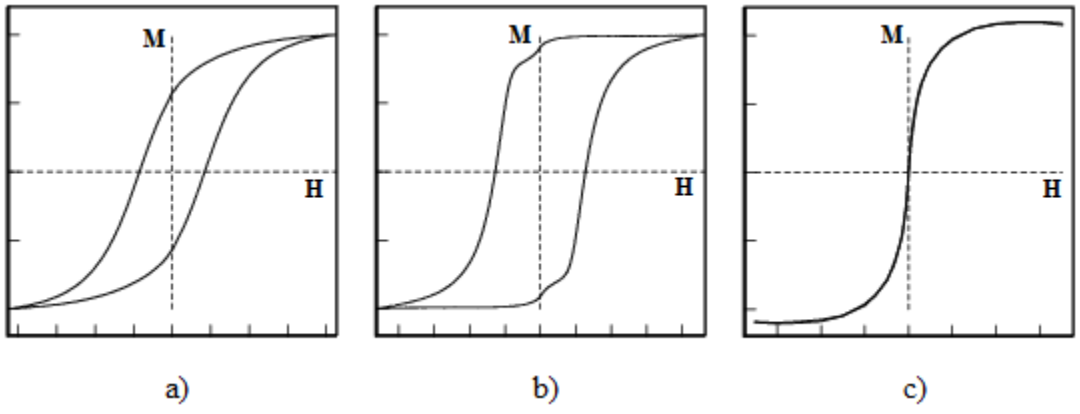


Figure 4. a) Large particles hysteresis, b) Small particles hysteresis and c) Smaller particles hysteresis

### 4.3.2. Relaxation

The heat dissipation of superparamagnetic nanoparticles is due to the delay in relaxation of the magnetic moment. This relaxation can correspond either to the physical rotation of the particles themselves within the fluid, known as Brownian relaxation, or the rotation of the magnetic moments within each particle known as Néel relaxation.

The Brownian $\tau_B$ and Néel $\tau_N$ relaxation times are given by the following equations:

$$\tau_B = 4\pi\eta r_h^3/(kT) \tag{6}$$

$$\tau_N = \tau_0 \exp\left[\frac{KV}{kT}\right] \qquad (\tau_0 \sim 10^{-9} s) \tag{7}$$

where η is the viscosity of the fluid, T the temperature, and $r_h$ is the hydrodynamic radius which due to particle coating may be essentially larger than the radius of the magnetic particle core, *K* is the anisotropy constant, $V$ is the magnetic volume, and $\tau_0 = 10^{-9}\ s$. Since Brownian and Néel relaxation processes occur in parallel, the effective relaxation time is given by:

$$\frac{1}{\tau} = \frac{1}{\tau_B} + \frac{1}{\tau_N} \tag{8}$$

The relationship between magnetization M and the applied magnetic field H is expressed through the magnetic susceptibility $\chi$, which explains how magnetization varies with the applied magnetic field:

$$M = \chi H \tag{9}$$

The Brownian relaxation time is related to the applied magnetic field through the complex magnetic susceptibility and can be obtained from the following equation [45]:

$$\chi(f) = \frac{\chi_0}{1 - i2\pi f \tau_B} \tag{10}$$

where $\chi_0$ is the equilibrium susceptibility

The shorter relaxation time term dominates the effective relaxation time for a given particle size. $\tau_B$ is determined in part by the hydrodynamic properties of the fluid, while $\tau_N$ is governed by the magnetic anisotropy energy relative to thermal energy. Both Brownian and Néel processes may be present in a ferrofluid. In constrained (i.e., immobilized) superparamagnetic particles, such as iron oxide, only Néel relaxation occurs.

Relaxation times are temperature dependent. However for mild hyperthermia at near 42ºC, the relaxation time constants do not change by much, thus in this investigation the effect of small temperature elevations on the time constants are considered negligible.

The real and imaginary parts of the complex susceptibility can be expressed as shown in (11) and (12) [45]:

$$\chi' = \frac{\chi_0}{1+(\omega\tau)^2} \tag{11}$$

$$\chi'' = \frac{\omega\tau}{1+(\omega\tau)^2}\chi_0 \tag{12}$$

where $\omega = 2\pi f$, $\tau$ is the relaxation time. $\chi_0$ is the equilibrium susceptibility, and can be calculated from the following expressions:

$$\chi_0 = \chi_i \frac{3}{\xi}\left(coth\xi - \frac{1}{\xi}\right) \tag{13}$$

where the initial susceptibility $\chi_i$ is:

$$\chi_i = \frac{\mu_0 \emptyset M_d^2 V_M}{3k_B T} \tag{14}$$

and $\xi$ is the Langevin equation expressed as:

$$\xi = \frac{\mu_0 M_d^2 H_0 V_M}{k_B T} \tag{15}$$

where $\emptyset$ is the volume fraction of nanoparticles in the ferrofluid and $M_d$ is the domain magnetization of the nanoparticle, $H_0$ is the initial magnetic field, $V_M$ is the volume of nanoparticle and $k_B$ is the Boltzmann constant [45].

Figure 5 shows the real and the imaginary components of the susceptibility as given in (11) and (12). These components meet at the peak value of $\chi''$. The imaginary component of susceptibility is due to the phase difference between the applied magnetic field and the corresponding magnetization and therefore is responsible for generation of heat. $\chi''$ reaches its peak value when $\omega\tau = 1$.

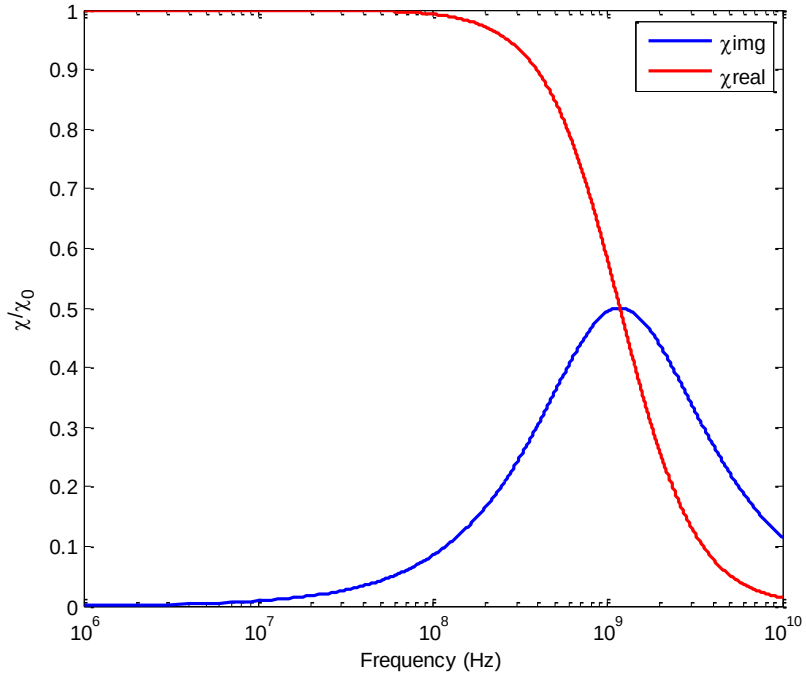


Figure 5. Real and imaginary components of the susceptibility vs. Frequency

To understand how the applied magnetic field causes a temperature increase in the magnetic nanoparticles, we look at the role played by $\chi''$.

The magnetic work done on the system is:

$$dU = H \cdot dB \tag{16}$$

where $H$ $(A/m^{-1})$ is the magnetic field intensity and $B(T)$ the induction. The fields are collinear and $H$ snd $B$ are magnitudes. Then, the relation between the magnetic field $H$ $(A/m)$ and the magnetic flux density (or induction flux) $B$ $(Wb/m^2)$, is:

$$B = \mu_0(H + M) \tag{17}$$

where $\mu_0$ is the permeability of free space and $M$ is the magnetization of the material ($Am^{-1}$) .

When the magnetization lags the field, the integration yields a positive result indicating conversion of magnetic work to internal energy [45], which can be expressed as:

$$\Delta U = -\mu_0 \oint M dH \tag{18}$$

where $\Delta U$ is the internal energy.

From (9), the magnetization as a function of time becomes:

$$M(t) = Re\left[\chi H_0 e^{i\omega t}\right] = H_0(\chi' \cos(\omega t) + \chi'' \sin(\omega t)) \tag{19}$$

where it is seen that $\chi'$ is the in-phase component, and $\chi''$ the out-of-phase component of $\chi$ and the internal energy can be expressed as:

$$\Delta U = \mu_0 H_0^2 \chi'' \int_0^{2\pi/\omega} sin^2(\omega t) dt \tag{20}$$

The volumetric power dissipation can now be expressed as:

$$P = \Delta U f = \mu_0 f H_0^2 \omega \chi'' \int_0^{2\pi/\omega} sin^2(\omega t) dt = \mu_0 f H_0^2 \pi \chi'' \quad (21)$$

where $f$ is the frequency.

Hence we see that when magnetic nanoparticles are injected into tumors, their magnetic properties are intensified, due to the complex susceptibility $\chi''$. Consequently, the external H field applied also plays an important role in the heating process.

From (21), it is observed that the power dissipation is proportional to the square of the amplitude of the H field intensity. Therefore, in the bioheat equation (3) written earlier, we include an additional term in $\mathrm{Q_{ext}}$ :

$$\rho_t c_t \frac{\partial T}{\partial t} = k \frac{\partial^2 T}{\partial x^2} - \omega_b \rho_b c_b (T - T_a) + Q_{met} + \frac{1}{2}\sigma_t |E|^2 + \pi \mu_0 \chi'' f |H|^2 \quad (22)$$

With nanoparticles injected into a tumor, the heating effect is produced by both the electric and magnetic fields generated by the external applicator; i.e., the heating effect produced by the external applicator in the tumor, depends not only of the square of E field but also of the square of H field.

When magnetic nanoparticles are present, the relation between the specific absorption rate (SAR) and the time rate of change of the temperature in the magnetic material is often expressed as:

$$SAR = \frac{cV_s}{m}\frac{dT}{dt} \quad (23)$$

where $c$ is the specific heat capacity of the sample, $m$ is the mass of the magnetic particles, $V_s$ is the total volume of the tissue containing the nanoparticle and $\frac{dT}{dt}$ is the temperature increment.

The specific absorption rate SAR is also proportional to the volumetric power dissipation P and can be written as:

$$SAR = \rho * P = \rho \pi \mu_0 \chi'' f |H|^2 \quad (24)$$

where $\rho$ is the density of nanoparticle.

# CHAPTER 5: MICROWAVE MAGNETIC FLUID HYPERTHERMIA MODELING

## 5.1. Introduction

The results for enhanced magnetic fluid hyperthermia using magnetic nanoparticles is presented for the case of a tumor in the breast tissue. The mathematical modeling is done using the Penne's bioheat equation. Simulations are carried out with HFSS and SEMCAD X [47]. The SAR values and the transient temperature are studied as a function of the nanoparticle characteristics, such as size, concentration etc. Experiments on phantoms breast and tumor tissue were conducted to validate the simulated results obtained.

## 5.2. Magnetic Fluid Hyperthermia Design Considerations

The model consists of a sphere of radius 10 cm representing a single homogeneous breast fat tissue. A tumor of 1 cm radius is embedded at the center of the sphere, at 5 cm from the surface. The magnetic nanoparticles, immersed in a ferrofluid and are specially coated to target and attach to the tumor tissue. The hyperthermia system is shown in Figure 6, where the model is illuminated at 2.45 GHz with a standard horn antenna.

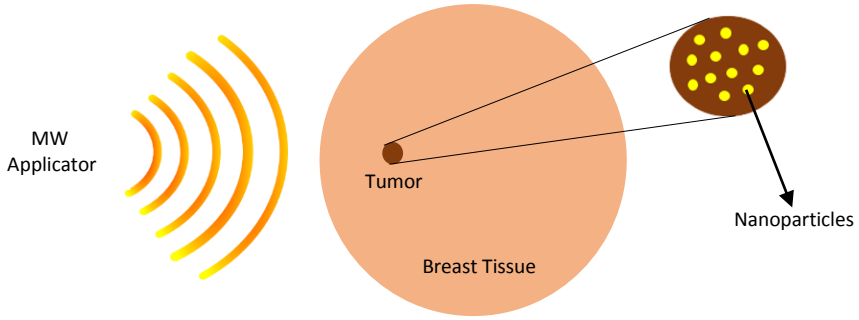


Figure 6. Hyperthermia system configuration

The electric properties of human breast tissue and tumor tissue such as dielectric constant and conductivity properties used in the model were assigned according to [12] and the SEMCAD X software database [47] and [48]. Table 3 lists these values.

Table 3. Electrical properties of human tissues

| Tissues | $\varepsilon_r$ | $\sigma$ (S/m) |
|---|---|---|
| Breast Fat | 5.28 | 0.105 |
| Tumor | 60.26 | 1.21 |

### 5.3. Heat Generation

With nanoparticles of concentration $n$ and radius $r$, the heat generation in tumor will be:

$$Q_{ext2} = \left(\frac{4}{3}n\pi r^3\right)\pi\mu_0\chi^{"}f|H|^2 \qquad (25)$$

where $n$ is the concentration of the nanoparticles in tissue, $r$ is the radius of the nanoparticle, $\chi^{"}$ is the magnetic susceptibility and $f$ is the frequency.

To determine the transient temperature, as discussed in Chapter 4, the Penne's bioheat equation in healthy tissue will be:

$$\rho_t c_t \frac{\partial T}{\partial t} = k\frac{\partial^2 T}{\partial x^2} - \omega_b \rho_b c_b (T - T_a) + Q_{met} + \frac{1}{2}\sigma_t |E|^2$$

and the Penne's bioheat equation with nanoparticles in the tumor tissue will be:

$$\rho_t c_t \frac{\partial T}{\partial t} = k\frac{\partial^2 T}{\partial x^2} - \omega_b \rho_b c_b (T - T_a) + Q_{met} + \frac{1}{2}\sigma_t |E|^2 + \left(\frac{4}{3}n\pi r^3\right)\pi\mu_0\chi^{"}f|H|^2$$

The computed heat generation produced by the nanoparticles is included as the heat source in the bioheat equation to compute the temperature distribution in the model.

Table 4 shows the thermal properties considered for healthy and tumor tissues for use in the bioheat equation, according to [47].

Table 4. Thermal properties of human and tumor tissues

| Tissues | ρ (kg/m$^3$) | C (J/kg.°C) | K (W/m.°C) | $Q_{met}$ (W/kg) | B (W/m$^3$.°C) |
|---|---|---|---|---|---|
| Breast Fat | 916 | 2524 | 0.25 | 0.328 | 916 |
| Tumor | 1043 | 3621 | 0.5 | 6.807 | 35 |

### 5.4. Simulation

SEMCAD X, a commercial finite-difference time-domain (FDTD) based program for analysis of bio-electromagnetic effects along with the software HFSS was used to obtain the SAR values and the transient temperatures. The propagating electromagnetic waves are generated by an antenna placed near the body with maximum radiation pointing towards the body. In SEMCAD X, the electric field and magnetic field strengths in the human tissue are obtained with a sensor called the overall field sensor. SEMCAD X provides thermo-simulation where the complete thermal profile of human tissues is obtained taking the blood flow, i.e. the density of blood, blood perfusion rate and the blood specific heat, into account. The program allows the determination of SAR values and temperature distribution by using thermosensors. Several thermosensors can be placed along the model to record the temperature. For the enhanced hyperthermia study in this model the blood flow was not taken into account.

The specific absorption rate and the temperature profile in the model were first evaluated without injecting any nanoparticles into the tumor. The electromagnetic source was set to 50 V

and a tumor of 1 cm was located inside the breast phantom at a depth of 50 mm. the total treatment time is 1800 sec. The model used in SEMCAD X is shown in Figure 7.

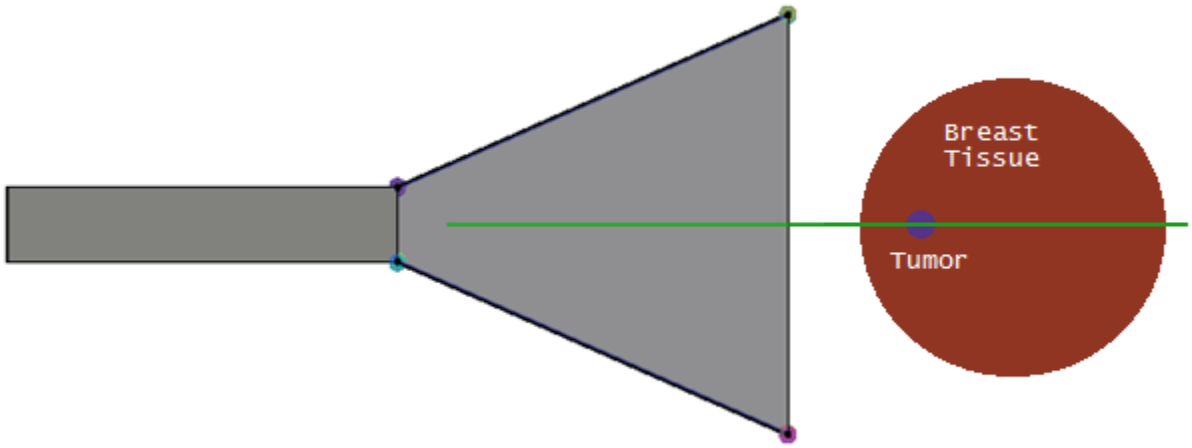


Figure 7. Breast tissue model in SEMCAD X

### 5.5. Temperature Measurements using SEMCAD X

Three temperature sensors were used to record temperature increase as the breast tissue was illuminated by the electromagnetic wave. These temperature measurements were recorded inside the healthy breast phantom and in the ferrofluid with nanoparticles. One sensor was placed at the center of the tumor, the remaining two sensors were placed at 2.5 and 5 cm from the first sensor, respectively.

Figure 8 shows the temperature distribution in the breast model obtained from SEMCAD X. With no nanoparticles present, there is an insignificant temperature increase in the tumor to cause any damage to the cells. Here, the temperature peaks occur right at the boundary of the

tissue, where the potential has the largest gradient, and therefore the electric field strength appears the maximum in this area.

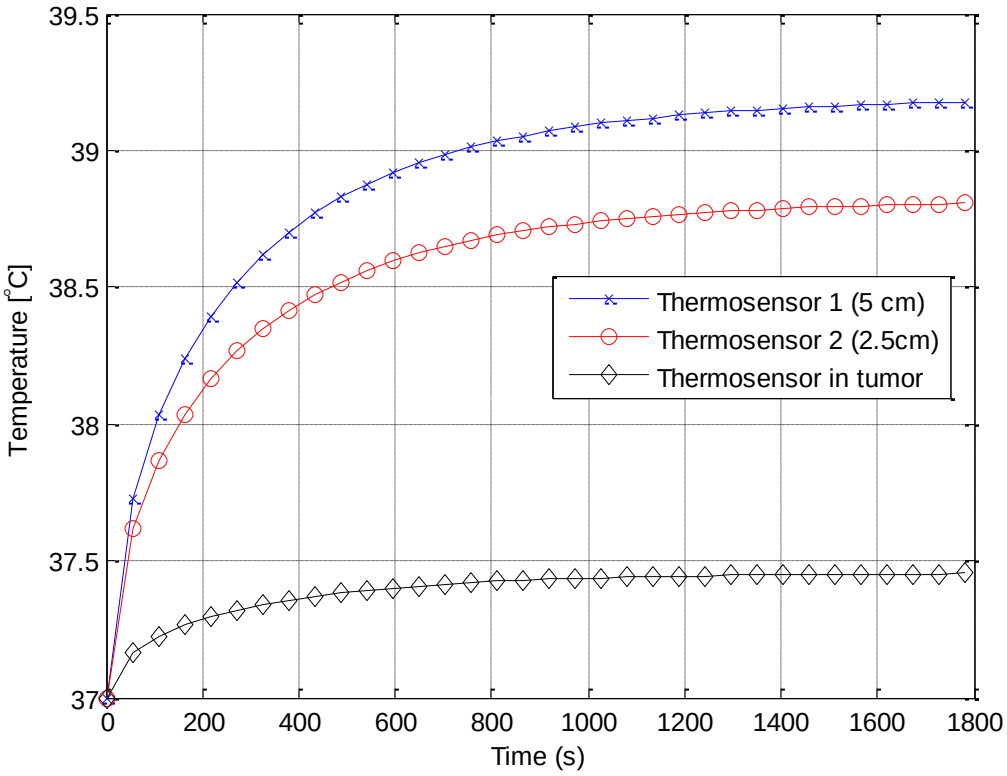


Figure 8. Tempertaure distribution during hyperthermia without nanoparticles

Magnetic iron oxide nanoparticles, with the properties listed below [49-50] were injected into the tumor and the transient temperature was once again studied:

$density\ (\rho) = 5180\ kg/m^3$

$concentration\ (n) = 1x10^{21}\ m^{-3}$

$thermal\ conductivity\ (K) = 40\ W/m \cdot ℃$

$specific\ heat\ (C) = 4000\ J/kg \cdot ℃$

$Saturation\ Magnetization\ (M) = 52\ emu/g$

$radius\ (r) = 18\ nm$

$magnetic\ susceptibility\ (\chi^{"}) = 65$

These results are shown in Figure 9. The temperature at the tumor tissue region is now at 43.3°C, which is the required temperature for hyperthermia treatment.

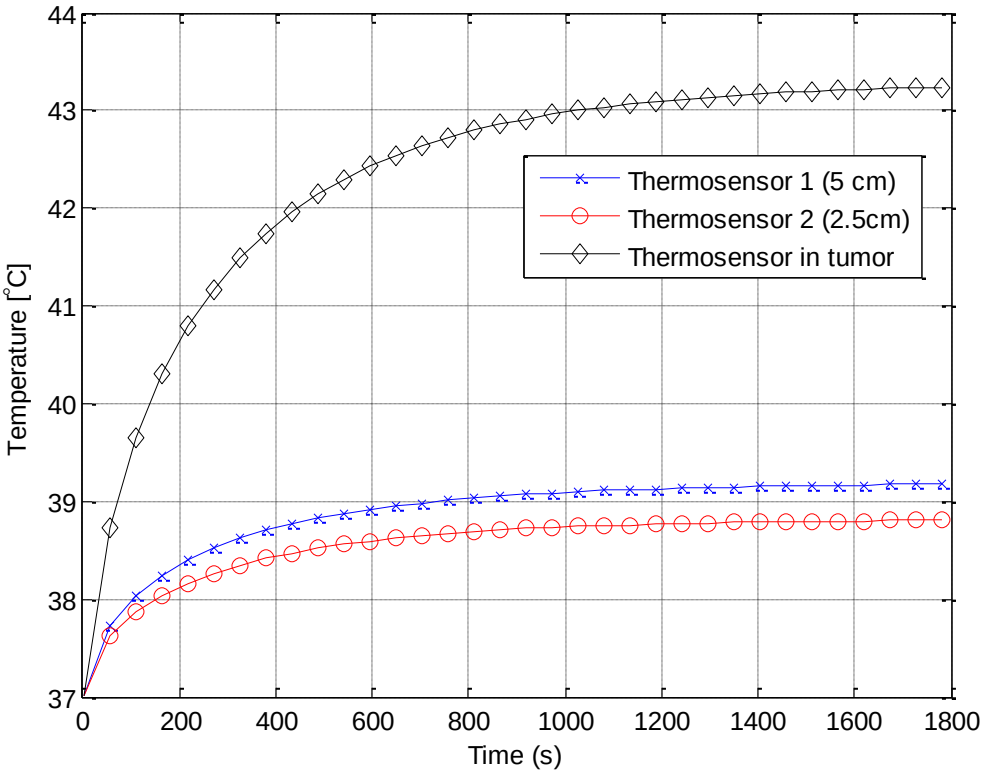


Figure 9. Tempertaure distribution during hyperthermia with nanoparticles

The temperature is highest at the breast tissue close to the electromagnetic applicator and drops as the distance from the applicator increases. At the tumor location, there is once again an increase in the temperature due to the heat generated by the nanoparticles, in the healthy tissue the blood flow is not restricted in the capillaries and this allows helps in maintaining the healthy temperature. On the other hand, in cancerous tumors the blood flow is restricted significantly also contributing to a rise in temperature. This is show in Figure 10.

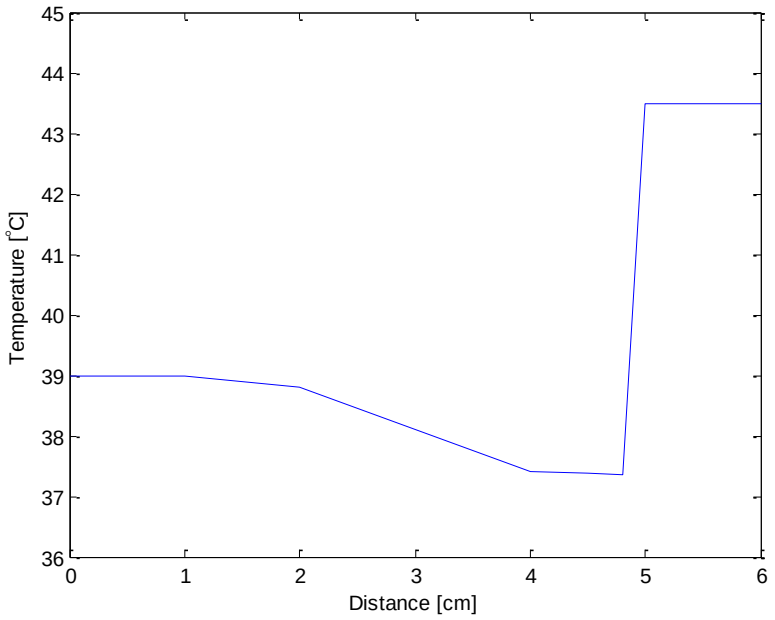


Figure 10. Time temperature increase in the tissue as function of distance from the applicator

### 5.6. Effect of Nanoparticle Characteristics in the Transient Temperature in the Tumor

For an exposure time of 1800 seconds, various characteristics of the nanoparticles such as their size, magnetic susceptibility and concentration were studied to see their effect on the transient temperature, once they were introduced into the tumor.

### 5.6.1. Nanoparticle Size

To test the effect of the nanoparticle size on the tumor heating nanoparticles sizes of 5 nm, 9 nm and 18 nm were considered. The results from the transient temperature using SEMCAD X are shown in Figure 11. It is found that a higher tumor temperature can be induced with the particle radius of 18 nm. Larger nanoparticles sizes were not considered in this study since, because when the particle size becomes much larger, they lose their superparamagnetism characteristic and thus lowering the heat generation capability [51].

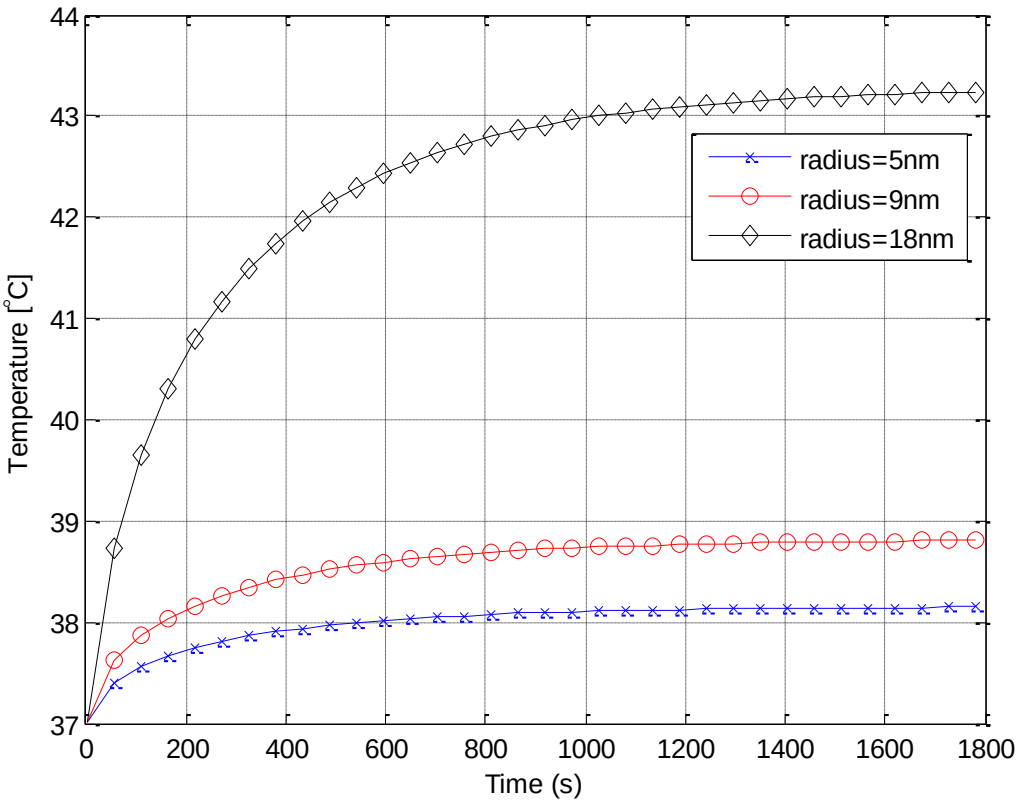


Figure 11. Transient temperature in the tumor for different nanoparticles sizes

Particles with 18 nm diameter showed the highest heating ability obtaining a temperature rise ΔT = 6 °C and reaching the target temperature of 43.3 °C. The other nanoparticles considered produced only a temperature raise in the range ΔT= 1 – 3 °C.

To explain this, we evaluated the relaxation times Brownian $\tau_B$ and Néel $\tau_N$ in section 4.3.2 equation (8). Here, the Brownian relaxation time $\tau_B$ is neglected because it is much larger than the Néel $\tau_N$ relaxation time in living tissue that has large viscosity. We know that the maximum loss is obtained when $\omega\tau \cong 1$ at a critical volume size. At frequency ${}^{\omega}/_{2\pi} = 2.45\ GHz$, the optimum relaxation time is $\tau = 4 \times 10^{-10}$ s, which is realized, as shown in Figure 12, when r is around 18 nm. This coincides with our results. The nanoparticles with 9 and 5 nm radius, which have Néel relaxation time far from the optimum relaxation time, exhibit much weaker magnetic induction heating as compared to the 18 nm sized particles which has nearly optimum relaxation time.

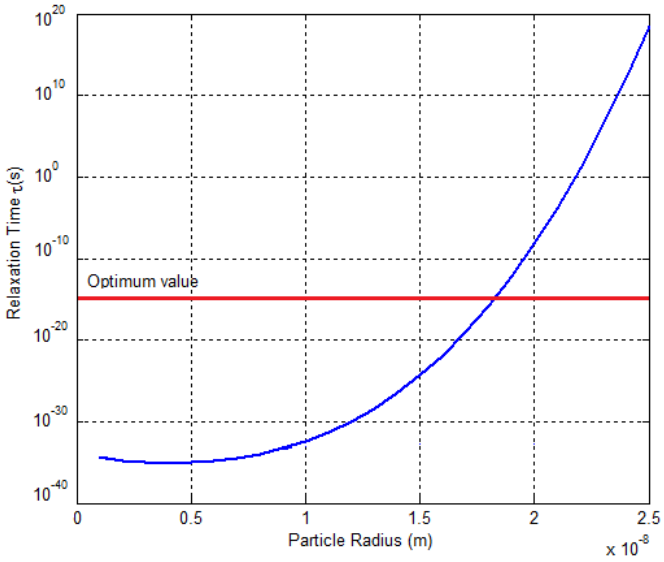


Figure 12. Néel relaxation time $\tau_N$ as a function of radius of the nanoparticle

### 5.6.2. Nanoparticle Susceptibility

Next, we consider the effect of the nanoparticle susceptibility on the heating behavior. Susceptibility values of 15, 35, 55 and 65 were considered and the results are shown in Figure 13. When the nanoparticle susceptibility is 65, the peak of the temperature in the tumor region is 43.3 °C, indicating that a higher susceptibility value provides the desired results for heating the tumor.

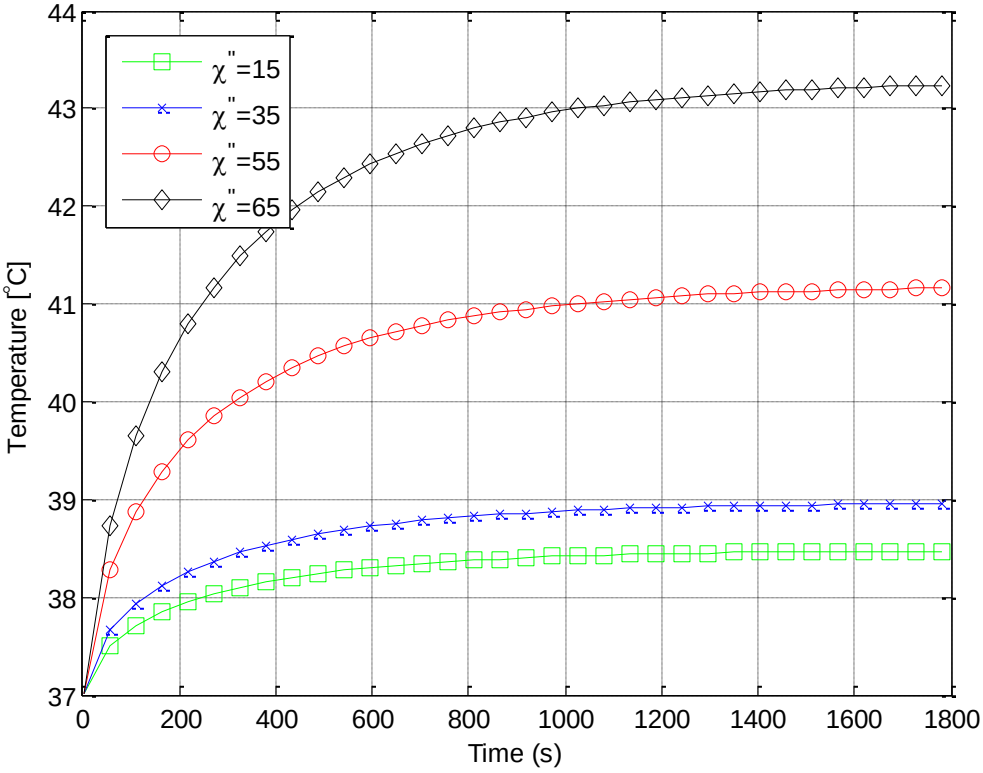


Figure 13. Transient temperature in the tumor for different nanoparticles susceptibilities

### 5.6.3. Effect of Nanoparticle Concentration on the Heating Behavior

Figure 14 shows the influence of the nanoparticle concentration on the increase in the tumor temperature. With a magnetic nanoparticles with a concentration equals of 60 $mg/ml$, we

see that the peak temperature in the tumor region is 68 °C. Such high temperatures can cause thermal injury to the surrounding tissue and are much higher than is needed for hyperthermia. A nanoparticle concentration of $40\,mg/ml$ provides the required temperature level for hyperthermia treatment for the exposure time considered.

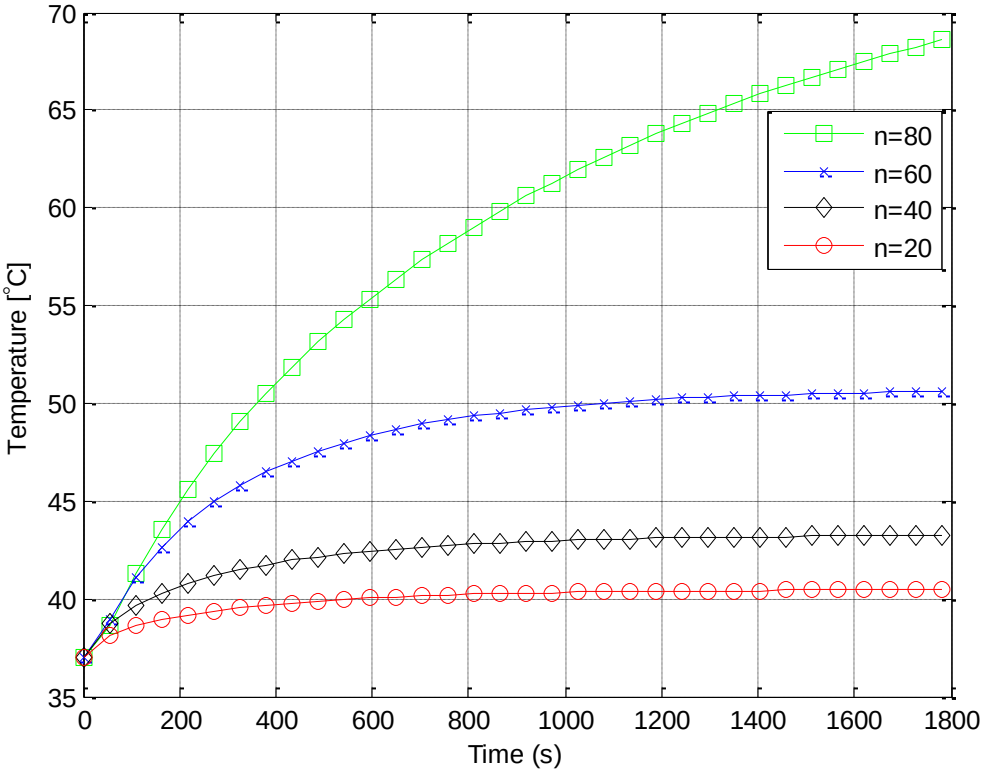


Figure 14. Transient temperature in the tumor with different nanoparticles concentrations

### 5.6.4. Optimization of Nanoparticle Concentration

Appropriately choosing the heating dose before performing the hyperthermia is essential for proper treatment planning. The relative importance of the heat source induced by the

nanoparticles and that in normal tissue can be evaluated through an analysis of equation (22) in section 4.3.2. The heat generation in tumor tissue with nanoparticles is given by:

$$Q_{tumor} = \left(\frac{4}{3}n\pi r^3\right)\pi\mu_0\chi^{"}f|H|^2 + \left(1 - \frac{4}{3}n\pi r^3\right)\frac{1}{2}\sigma_t|E|^2 \qquad (23)$$

According to [45], the amplitude of the magnetic field intensity can be expressed as:

$$H = \frac{1}{1+N(\chi)}\frac{E}{\pi\mu_0 f} \qquad (24)$$

Which indicates that for a spherical composite the demagnetizing factor of the composite tissue $N(\chi) = 1/3$.

In hyperthermia, the heat generated by the nanoparticle should always be larger in the tumor than that in healthy tissue. The specific power loss of the nanoparticles should be as high as possible in order to minimize the heating dose required for the treatment. A criterion to determine the minimum particle concentration for clinical application is proposed as:

$$\frac{3nr^3\chi^{"}}{4\mu_0 f} \geq \left(1 - \frac{4}{3}n\pi r^3\right)\frac{1}{2}\sigma_t \qquad (25)$$

Indicating that the particle concentration $n$ be as given below:

$$n \geq \frac{\frac{1}{2}\sigma_t}{\frac{3r^3\chi^{"}}{4\mu_0 f} + \frac{2\sigma_t\pi r^3}{3}} \qquad (26)$$

## 5.7. Experimental Results

### 5.7.1. Solid Phantom

In most instances, experiments cannot be done on human bodies and hence for medical research, phantoms are used. A phantom is prepared so as to simulate actual biological tissues and allows one to study interactions between applied electromagnetic fields and the human body. Phantoms provide a stable, controllable environment for such studies. Phantoms can be prepared to simulate the whole body or specific tissues or organs in the body. The ways to prepare these phantoms are available in the literature.

A human breast phantom using corn oil (150 ml), tri-distilled water (50 ml), neutral detergent (30 ml), and agarose (4.5 g) [52] was made to simulate the relative permittivity and electrical conductivity [12] of human breast fat tissue at 2.45 GHz. Figure 15 shows the phantom breast tissue fabricated. The relative permittivity of breast fat is 5.28 and electrical conductivity is 0.105 S/m for 2.45 GHz. The dielectric constant of the breast phantom was measured using a ring resonator [53] and was found to be 5.1 and 0.13 S/m, agreeing well with the reported dielectric constants.

The tumor phantom was made using tri-distilled water (100 ml), ethanol (60 ml), and NaCl (1g) mixed together and heated at $\sim 80^{\circ}$C for 5 minutes. The measured permittivity for the phantom mimicking the tumor was 59, which agrees well with the reported value of 60.

Figure 15. Solid phantom simulating the human breast tissue

Nanoparticles of 39 mg/mL were injected into small spheres of agarose (~10mm diameter), made with 0.006 g/mL of agarose to simulate the tumor tissue, as shown in Figure 16. The agarose sphere was then placed inside the breast phantom at a 5 cm depth before it got totally solidified.

Figure 16. Ferrofluid conatining the nanoparticles and tumor phantom

### 5.7.2. Measurement Setup

The breast phantom was illuminated at 2.45 GHz with a standard horn antenna, placed at 6 cm from the phantom, for 30 minutes, as shown in Figure 17. Thermometers were used to measure the temperature in the phantom breast and tumor.

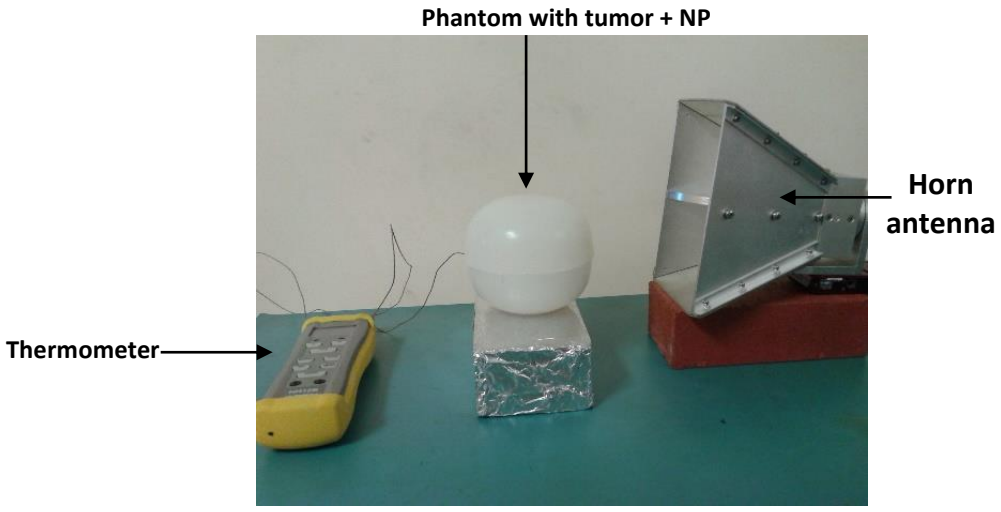


Figure 17. Measurement setup

### 5.7.3. Temperature Measurements

The phantom was placed just above the central point of the aperture of the horn antenna and the temperature was measured using thermometers placed in the tumor and at two locations in the breast phantom 2.5 cm and 5 cm from the tumor. The input power used in each exposure to the electromagnetic field was 1 W and each exposure was for 1800 s. The initial temperature of both the healthy and the tumor phantom was the room temperature of 21 °C, and the temperature increment $\Delta T$ was measured with the thermometer.

First, temperatures were taken in the phantom without nanoparticles injected. The results are shown in Figure 18. It can be seen that there is no significant change in temperature $\Delta T$.

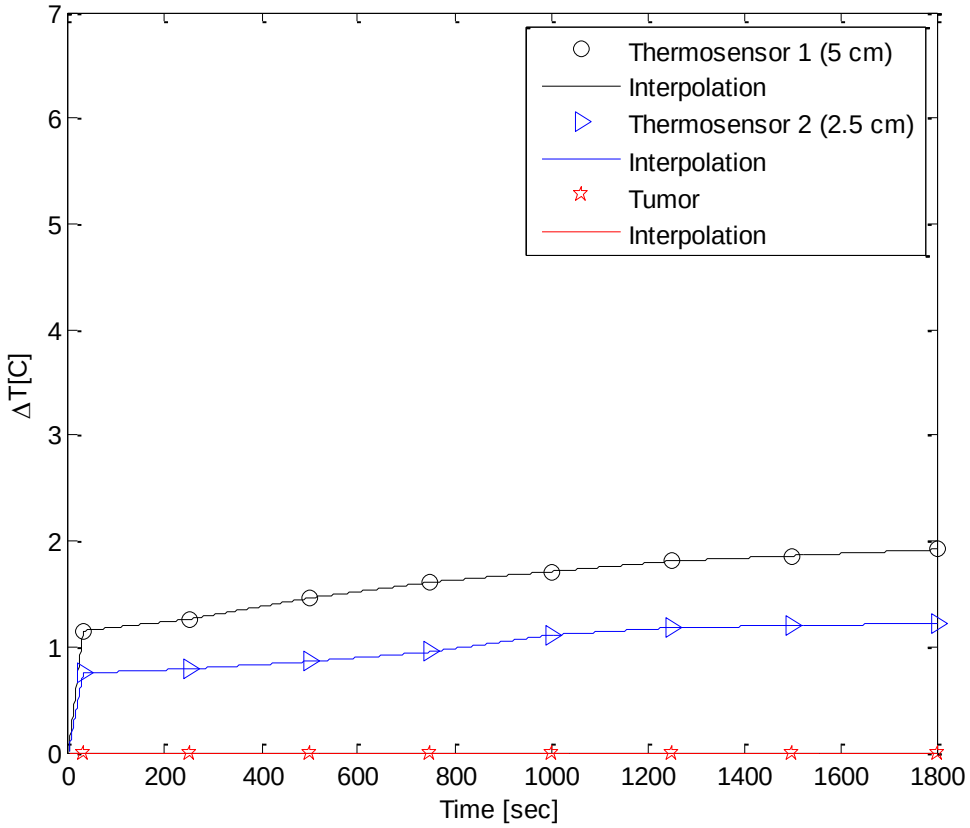


Figure 18. Temperature in phantom without nanoparticles

Then, the temperature was measured at the same locations after injecting nanoparticles into the tumor. The results obtained are presented in Figure 19.

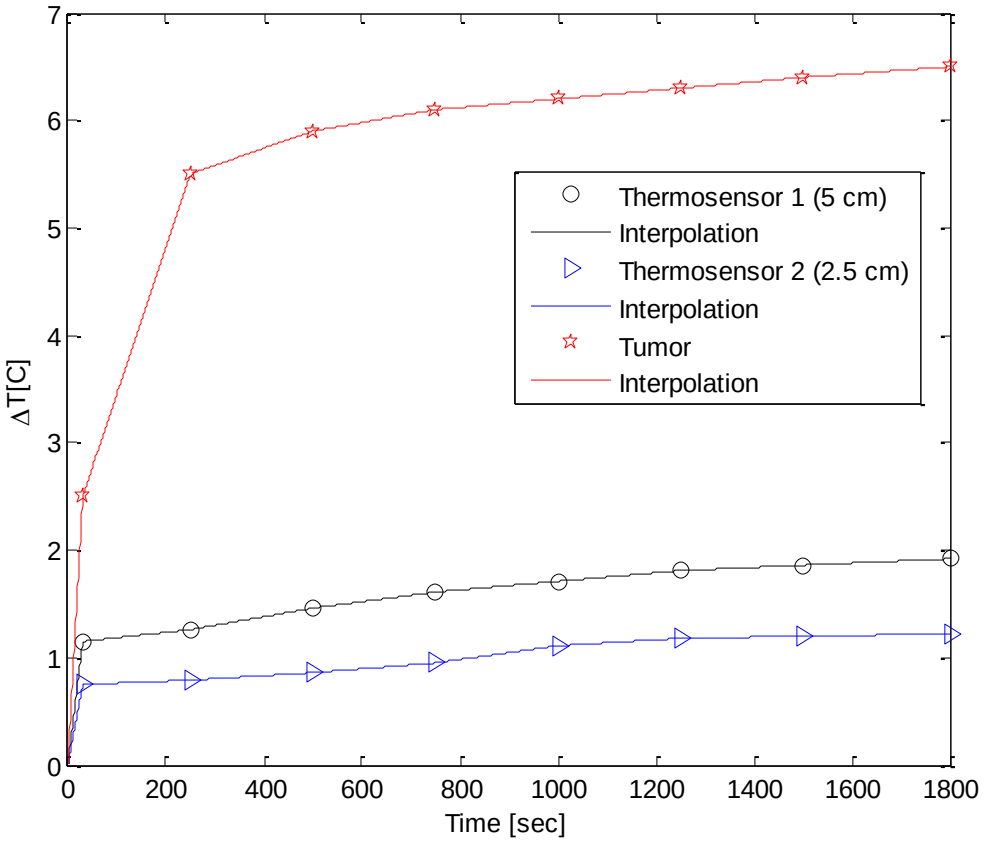


Figure 19. Temperature in phantom with nanoparticles

The measurements validate the results obtained with the simulations. There is an increase in the tumor around 6 - 7°C, which indicates that the nanoparticles exhibit a highly focused heating in the tumor tissue region, which is much higher than that in the surrounding healthy tissue.

# CHAPTER 6: MAGNETIC FLUID HYPERTHERMIA INCORPORATING BLOOD FLOW

## 6.1. Introduction

The response of human tissues to hyperthermia treatment is influenced by a number of physical, physiological, biochemical, and immunological factors which determine its effectiveness. A knowledge of these influences is essential to improve the results presently obtained by tumor treatment with hyperthermia alone or in combination with radiotherapy or chemotherapy.

The major physiological factor that has been of great interest to a number of investigators is the blood flow [54-57]. It is known that temperature distributions within the tumor and surrounding normal tissue during hyperthermia are influenced primarily by convective heat transfer between the blood and tissue bed. The local blood perfusion rate plays a major role during hyperthermia [57]. The blood flow causes a cooling effect in the tissues.

When hyperthermia is used in combination other cancer treatments, such as radiotherapy and chemotherapy, the sequence of therapy is governed by the role blood flow plays in each of these modalities.

## 6.2. Blood Perfusion in Humans

Studies on blood perfusion in tissues have proven that the blood perfusion in tumors varies significantly with type, phase and size of the tumor. Also, the greater the blood perfusion rate of the tissue is, the greater the cooling effect. An important point is that the significant

differences between the blood perfusion rate of normal tissue and that of tumors causes selective heating of tumors in hyperthermia [56]. Table 5 shows the typical blood perfusion rate for various tissues and organs [58].

Table 5. Blood perfusion in human tissues

| Tissue Type | Anatomical Location or Organ | Specific Blood Flow Rate ($mm^3$/sec-gm) |
|---|---|---|
| Adipose tissue | Abdomen | 0.507 |
| | Thigh | 0.33 |
| Bone | Humerus, marrow flow only | 0.055 |
| Connective tissue | Typical, basal | 0.50 |
| Joint | Knee | 0.487 |
| Muscle | Calf, anterior, (max) | 0.46 (9.15) |
| | Forearm, (max) | 0.53 (8.38) |
| | Thigh, anterior, (max) | 0.43 (6.00) |
| | Typical, basal (max) | 0.50 (10.0) |
| Organ | Brain, basal (max) | 9.0 (18.3) |
| | Gastrointestinal tract, basal (max) | 6.7 (26.7) |
| | Heart, basal (max) | 13.3 (64.0) |
| | Kidney, basal (max) | 67 (100) |
| | Liver, basal (max) | 9.6-14.2 (54.5) |
| | Lung, basal (max) | 90 (490) |
| Skin | Abdomen | 1.44 |
| | Arms | 1.40 |
| | Calf | 1.77 |
| | Face | 11.7 |
| | Foot | 2.38 |
| | Forearm | 9.22 (46.7) |
| | Hands | 3.35 |
| | Head | 7.15 |
| | Thigh | 1.6 |
| | Thorax | 6.45 |
| | Typical | 1.7 (25.0) |

In liver tissue, which we will study here, the lower blood perfusion in tumorous tissues results in some protection for the surrounding healthy tissue during local hyperthermia treatment. The normal liver receives two-thirds of its blood supply from the portal vein system, whereas tumors in the liver derive virtually all of their blood supply from the hepatic arterial system.

Thus, for hepatic tumors, substances injected into the hepatic arterial system will be preferentially delivered to the liver tumor [59]. Hence, the use of magnetic nanoparticles by injecting them into the tumor via arterial embolization, provides an effective way to kill tumor cells.

In arterial embolization, also known as trans-arterial embolization (or TAE), a catheter (a thin, flexible tube) is inserted into an artery through a small cut in the inner thigh and threaded up into the hepatic artery in the liver. A dye is injected into the bloodstream so that the doctor monitor the path of the catheter via angiography. The nanoparticles can then be injected through the catheter.

### 6.3. Magnetic Fluid Hyperthermia Design Incorporating the Blood Perfusion

The use of enhanced hyperthermia with magnetic nanoparticles (also referred to as magnetic fluid hyperthermia) was studied for liver tumor by incorporating blood perfusion. Case simulations were performed using a male human model [47], shown in Figure 20, provided by SEMCAD X. SEMCAD X provides the complete 2.5D rendering of a typical adult male human body including bones, skin, heart, brain (grey matter), brain (white matter) etc. Each tissue and organ can be assigned relative permittivity and conductivity values that can be used to determine an objects complex permittivity and loss tangent. For accurate modelling at a given frequency, *f*, the Gabriel tissue parameters [12] can be calculated and imported into SEMCAD X. Typically for any body part the conductivity increases as the frequency increases and the relative permittivity decreases as the frequency decreases.

Figure 20. Human model in SEMCAD X

In this research, liver tumor models with the different blood perfusion rates labeled as models 1–5, as shown in Table 6, were studied. The blood perfusion rates were assumed to be homogeneous in the tumor and to be 100% (model 1), 75% (model 2), 50% (model 3), 25% (model 4) and 5% (model 5) of that of the liver. Model 5 has the typical blood perfusion rates for the tumor and normal tissues reported in literature [58]. Also, the blood perfusion rates of these models were assumed to be unchanged with changes in temperature. This assumption is made to simplify the comparison between the effects of the ratio between the normal and tumor tissue blood perfusion rates.

Table 6. Models with different blood perfusion rates

| Model | Tumor Blood Perfusion (ml/min/kg) | Liver Blood Perfusion (ml/min/kg) |
|---|---|---|
| 1 | 600 | 600 |
| 2 | 450 | 600 |
| 3 | 300 | 600 |
| 4 | 150 | 600 |
| 5 | 30 | 600 |

For this study, the liver and tumor are illuminated at 2.45 GHz with a standard horn antenna placed close to the surface of the body. A 1 cm tumor size is located inside the left lobe of the liver at approximately 50 mm from the surface. A ferrofluid containing iron oxide nanoparticles of concentration 40 mg/mL was injected into the tumor.

### 6.4. Simulated Transient Temperature

In SEMCAD, X six temperature sensors were used to record the increase in temperature. One sensor was placed at the center of the tumor, the remaining sensors were placed in the healthy liver tissue at 0.5, 2, 3, 4 and 5 cm from the tumor.

The temperatures obtained from the simulation by the sensors for the models 1-5 considered, are shown in Figures 21-25.

Figure 21 shows the transient temperature in model 1 where the blood flow in the tumor tissue is equal to that in the healthy liver, the temperature reaches a value of 37.5 °C after 1800 sec of exposure to the electromagnetic radiation. Since the blood perfusion in the tumor was equal to that of the healthy liver, selective heating of the tumor was difficult.

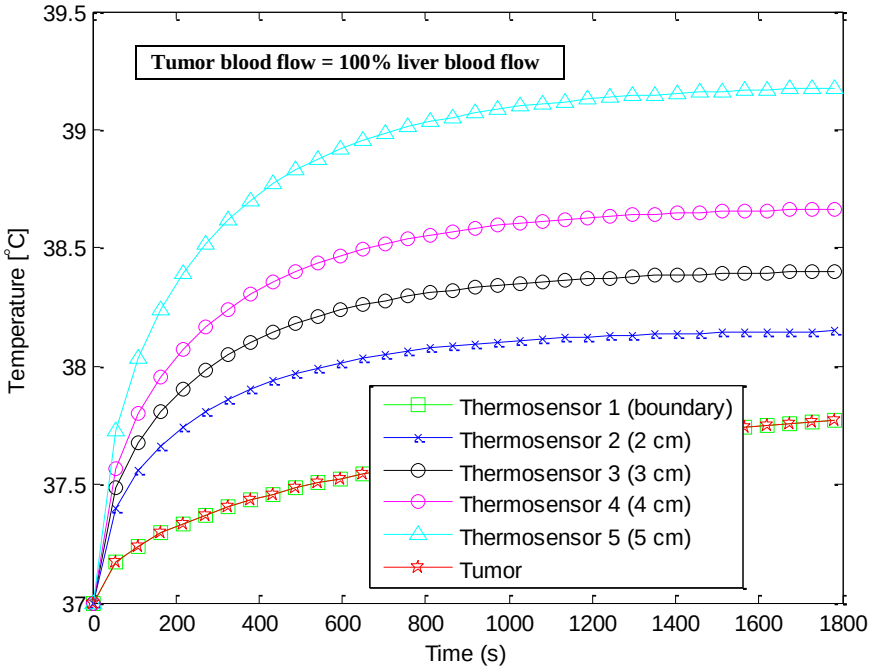


Figure 21. Transient temperature in the l.iver model – Blood perfusion rate 100%

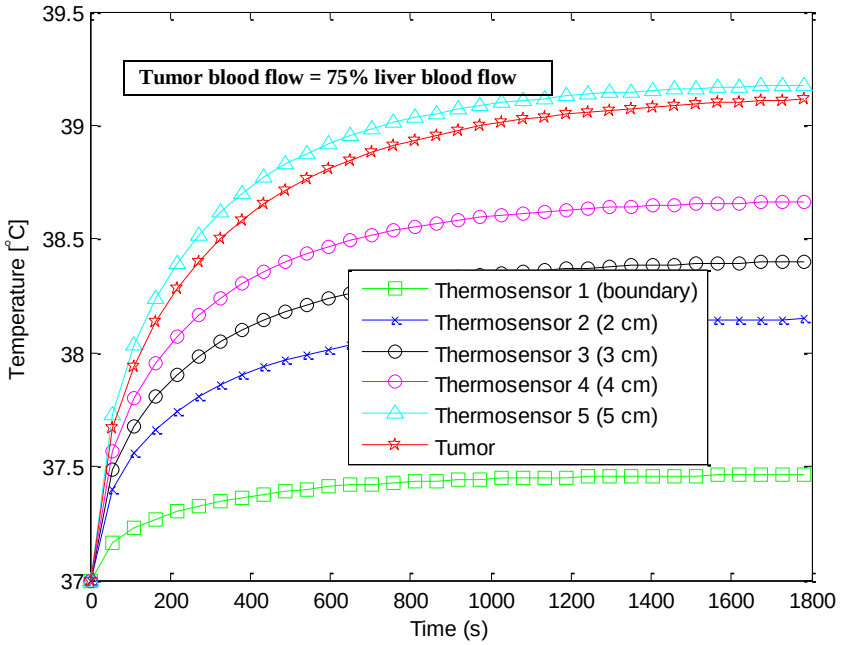


Figure 22. Transient temperature in the l.iver model – Blood perfusion rate 75%

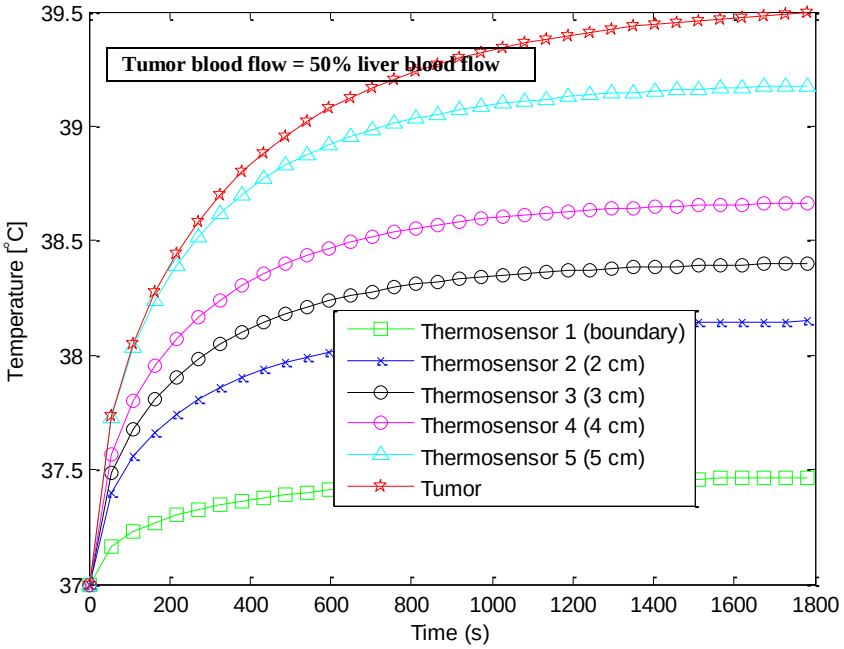


Figure 23. Transient temperature in the liver model – Blood perfusion rate 50%

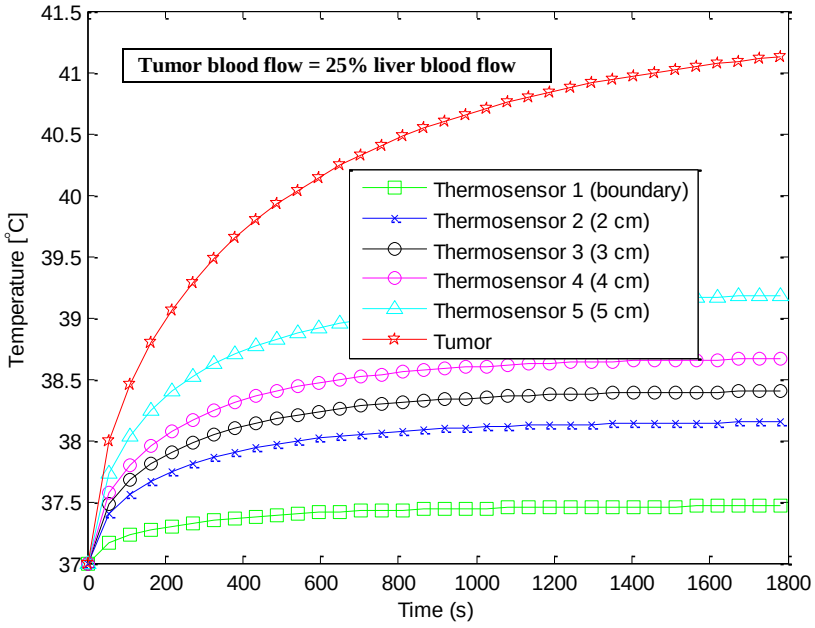


Figure 24. Transient temperature in the l.iver model – Blood perfusion rate 25%

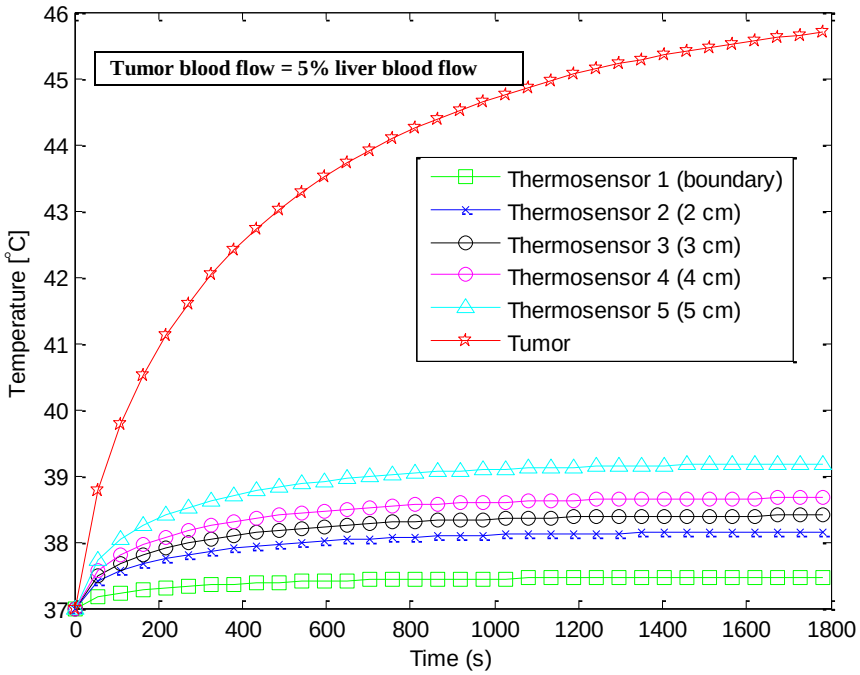


Figure 25. Transient temperature in the l.iver model – Blood perfusion rate 5%

In models 1– 4, with blood perfusion rates 100% to 25%, the lower blood perfusion in the tumors makes selective heating of the tumors easier. The healthy tissue does not shown an increased temperature. This is seen in Figures 21-24.

A comparison of the resultant tissue temperatures using models 1–5 indicates that temperatures in the tumor reached 43 °C in model 5, with blood perfusion rate of 5%, as seen in Figure 25.

This reinforces the importance of taking the blood perfusion into account in hyperthermia treatment. The normal blood flow in the healthy tissues keeps their temperature from raising to high, dangerous levels.

Figure 26 is a comparative plot of the healthy tissue and the tumor for the models studied.

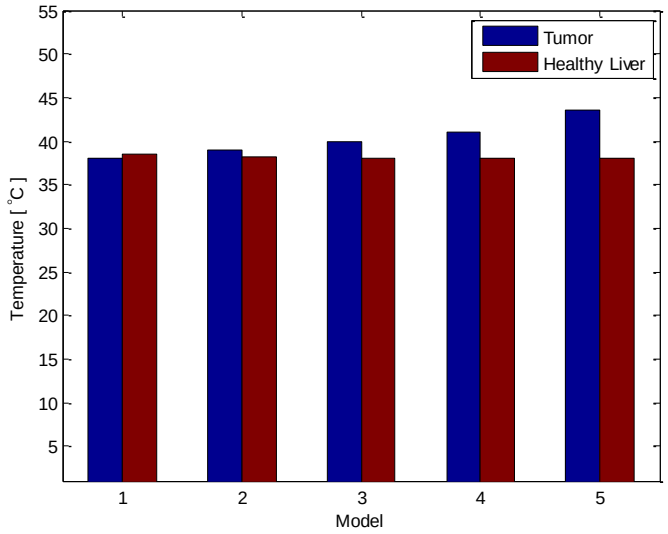


Figure 26. Temperature comparison in the tumor and healthy tissue

The SAR values, obtained from SEMCAD X, with blood perfusion included are shown in Figure 27. Once again, we see that in model 5 we get the high SAR values in the tumor, suitable for hyperthermia, while the healthy tissue SAR values stay at a safe level.

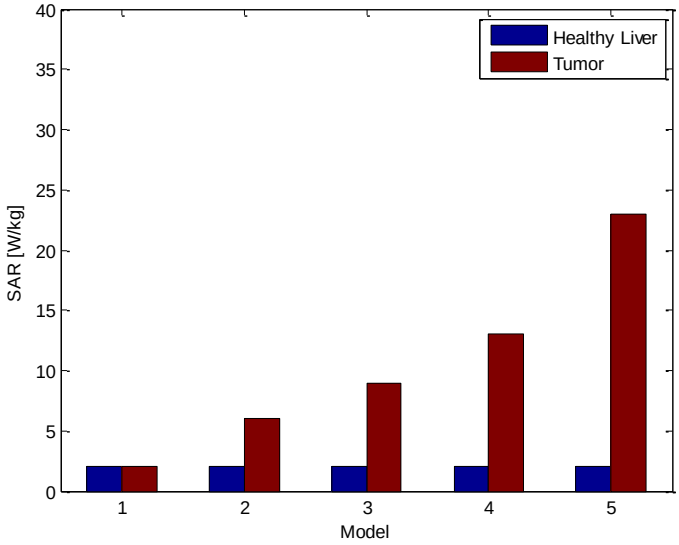


Figure 27. SAR comparison in the tumor and healthy tissue

Since the nanoparticle characteristics play a major role in the heating and the SAR for hyperthermia, a study of the effect of the nanoparticle concentration was done while including the blood perfusion. The particle radius was kept at 18 mm and the concentration were varied from 40 mg/mL to 60 mg/mL for each of the five models.

The results for the temperature in the tumor are shown in Figure 28. For model 5, with the lowest blood perfusion, a concentration of 40 mg/mL gives the desired temperature for hyperthermia.

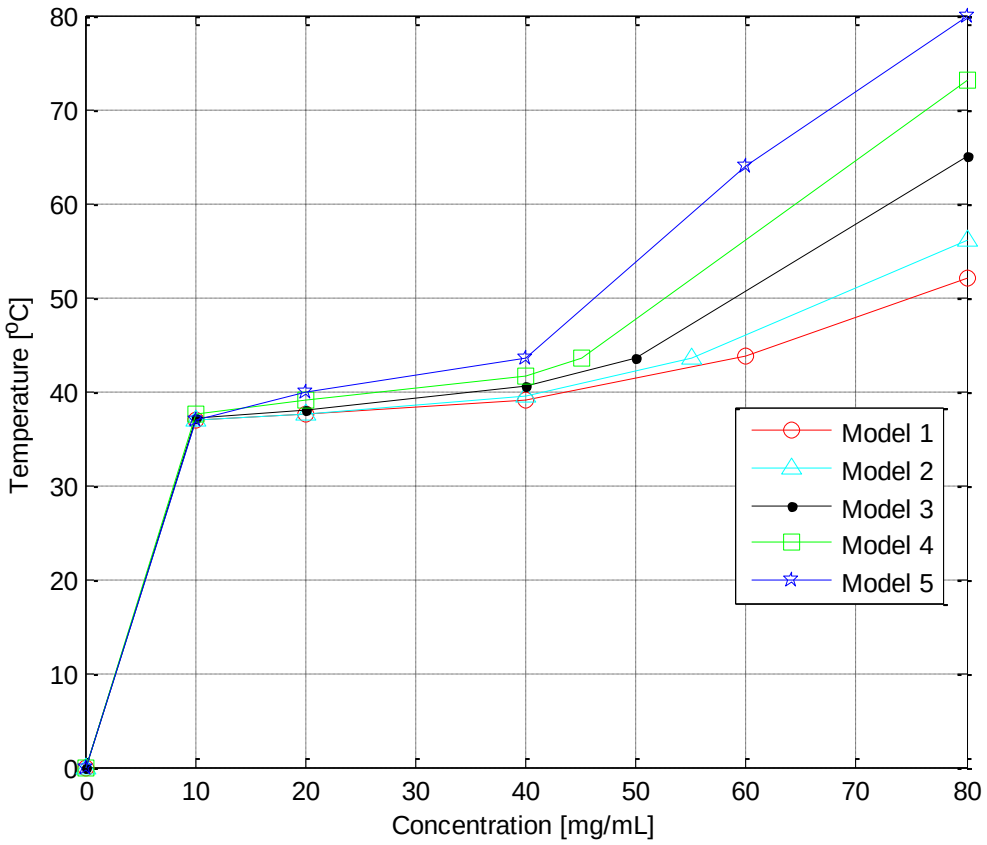


Figure 28. Temperature increase in the tumor as a function of nanoparticle concentration

### 6.5. Experimental Results using a Simplified Phantom

A simplified phantom model was made to carry out an experimental demonstration of the blood flow cooling effect in magnetic fluid hyperthermia. Figure 29 shows a cylindrical solid phantom liver size L= 6 cm and r = 8.5 cm. In this research, only the hepatic portal vein is considered. The hepatic portal vein is modelled as a cylindrical hole of 20 mm in diameter within the phantom. Saline solution poured through the liver phantom was used to simulate the cooling effect due to blood flow in the vein. The velocity of the saline solution is controlled by changing the diameter of a small hole in a rubber sheet placed at the bottom of the phantom.

The relative permittivity of this phantom is 47 and the conductivity is 2.2 S/m, which is equivalent to the electrical constants of human liver at 2.45 GHz. A 0.35 % saline solution is poured into the cylindrical hole modeling the hepatic portal vein. The value of the conductivity of the 0.35 % saline solution is 2.1 S/m, which is almost the same value that the human blood at 2.45 GHz. During the experiment, the saline solution is poured continuously. The permittivity of the tumor phantom was 59 and it was injected with iron oxide nanoparticle concentration of 40 mg/ml and placed at 50 mm from the surface.

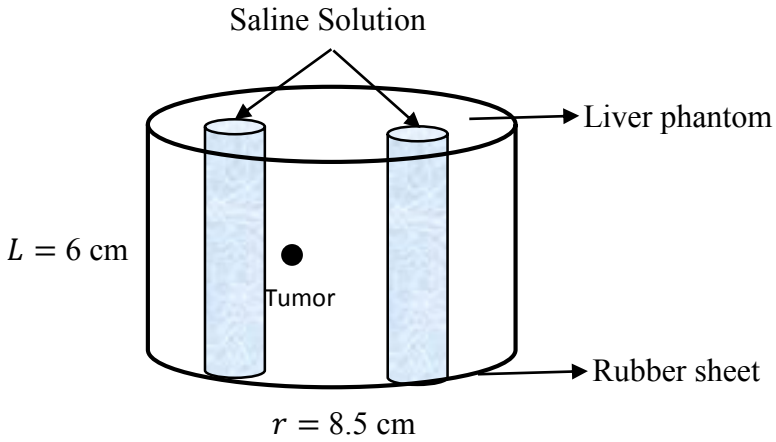


Figure 29. Simplified liver model

The blood flow can be expressed as:

$$Blood\ flow = \frac{pressure\ difference(\Delta P)}{resistance\ (R)} \tag{30}$$

The resistance blood flow depends on several factors including radius, length, and viscosity of the blood. The resistance can be expressed as:

$$R = \frac{\rho VD}{\mu} \tag{31}$$

where ρ is the blood density, V is the blood velocity, D is the diameter of the vein and μ is the blood viscosity [$\mu = 1.0 \times 10^{-6}\ J/kg \cdot K$].

In the experiment, the velocity of blood flow is varied by changing the diameter of the hole on a rubber sheet placed at the bottom of the phantom. For each one of the five models considered, a specific diameter of the hole was determined to obtain the corresponding blood flow velocity.

The total exposure time to the electromagnetic radiation was 1800 seconds, and the input power to the antenna was 1W. The initial temperature of the phantom and saline solution was close to the room temperature. Figure 30 shows the side view of the measurement setup,

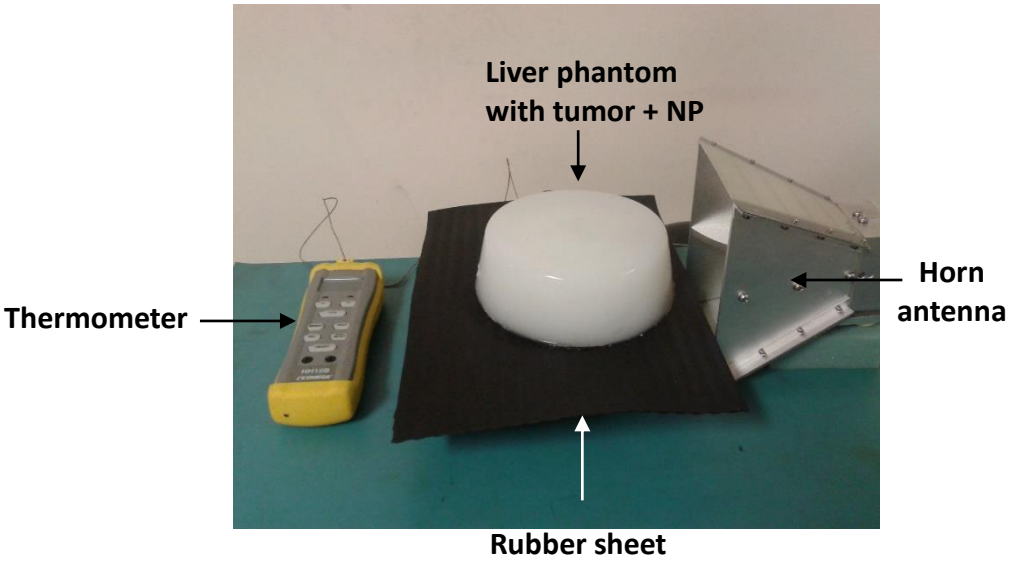


Figure 30. Liver phantom measurement setup – Side view

and Figure 31 is a top view of the liver phantom model showing the cylindrical holes to pour saline solution into.

Figure 31. Liver phantom model – Top view

### 6.6. Measured Temperatures

The phantom was placed in front of the 2.45 GHz horn antenna. The temperature was measured using the thermometer at five locations in the phantom and at one location in the tumor for a period of 1800 sec.

As mentioned earlier, the flow of the saline solution was controlled by changing the size of the hole on the rubber sheet at the bottom of the phantom, to model the five blood perfusion rates studied. The results are shown in Figures 32-36. The temperature increment ΔT °C above the normal temperature of 37 °C is shown. There is a noticeable increase in temperature for models 3 and 4, but once again, we see that in model 5, we obtain a ΔT between 5 and 6 °C which is what is desirable for hyperthermia. This agrees with the results obtained in the simulations.

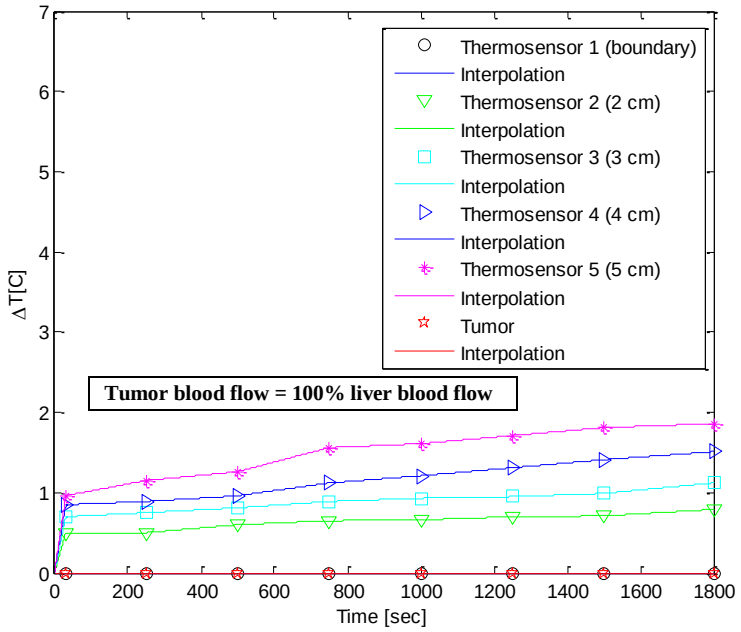


Figure 32. Temperature measured in healthy and tumor tissues in the model 1

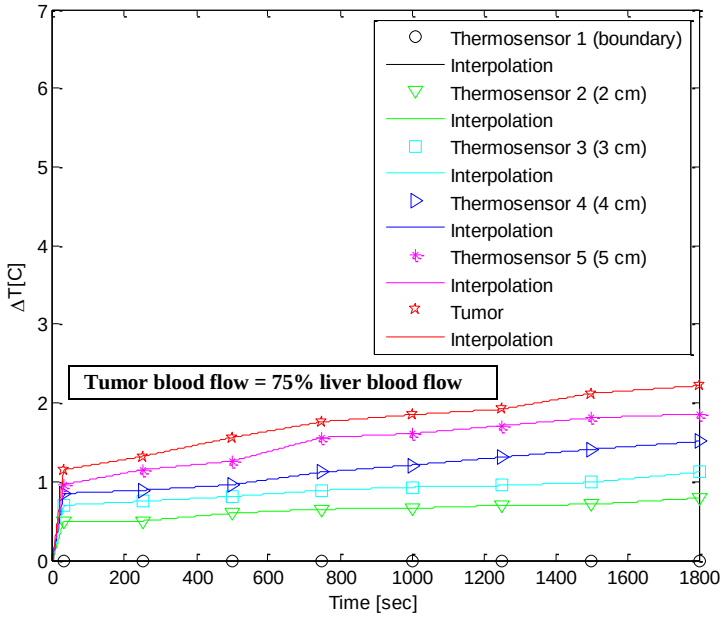


Figure 33. Temperature measured in healthy and tumor tissues in the model 2

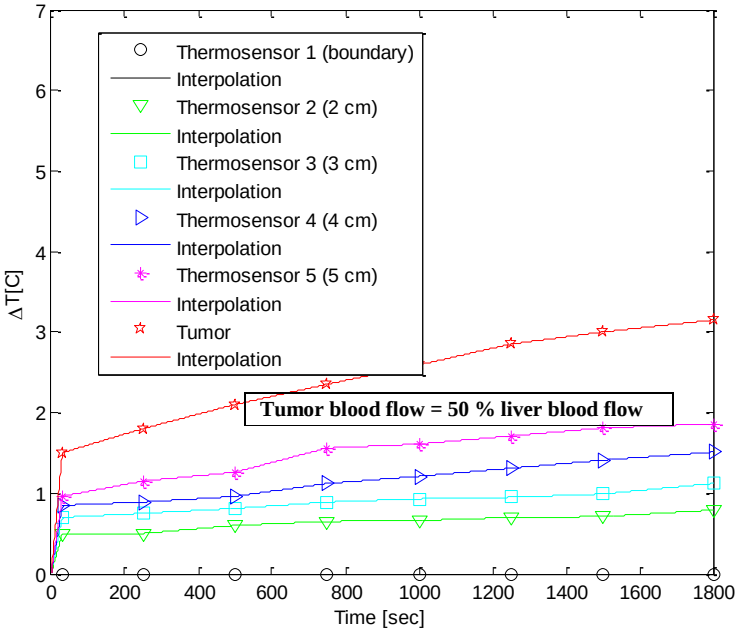


Figure 34. Temperature measured in healthy and tumor tissues in the model 3

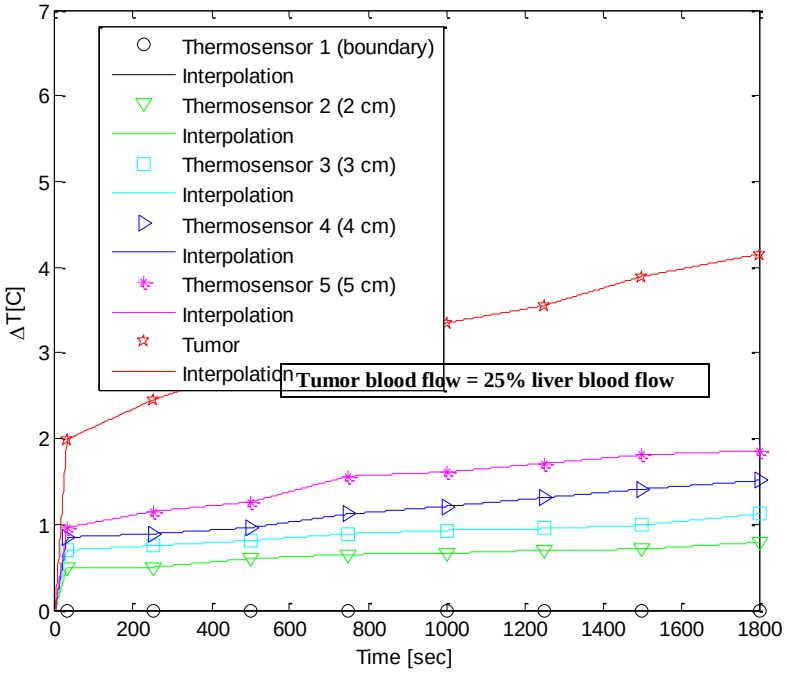


Figure 35. Temperature measured in healthy and tumor tissues in the model 4

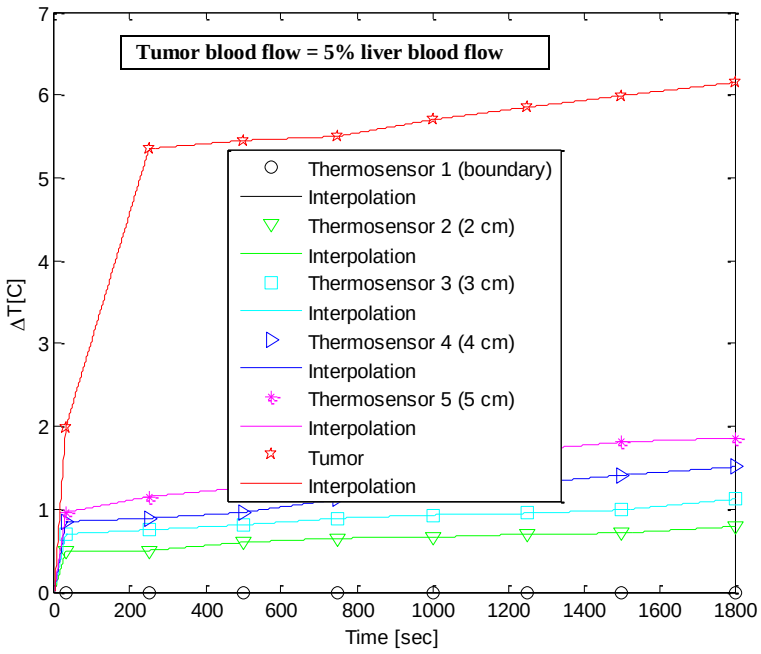


Figure 36. Temperature measured in healthy and tumor tissues in the model 5

### 6.7. Use of Magnetic Fluid Hyperthermia in Human Tissues

Although magnetic fluid hyperthermia is an effective cancer therapy, there are limitations that restrict its use to tumors growing in specific tissues in the body. These limitations include blood perfusion, which leads to large amount of blood removing heat from the tissue and the size the nanoparticles, which may restrict them from traveling into the smaller capillaries inside the tumor. Such restrictions prevent magnetic fluid hyperthermia from treating brain tumors where the blood-brain barrier does not allow effective injection of nanoparticles into the tumor. In lung tissues, the high blood perfusion results in rapid heat dissipation even before the nanoparticles can even reach the desired increased temperature needed to kill the cancerous cells. The low heat diffusivity and difficulty in pinpointing tumor locations in bone cancer also makes magnetic fluid hyperthermia a less effective treatment approach.

# CHAPTER 7: CONCLUSIONS

The technical challenge in hyperthermia treatment is to heat the tumor to the appropriate therapeutic temperature without causing damage to the surrounding healthy tissue. The results presented in this research show that conventional hyperthermia treatment can be enhanced through the use of magnetic nanoparticles.

A system with a microwave applicator at 2.45 GHz, magnetic nanoparticles and temperature monitoring sensors was modeled to effectively study hyperthermia treatment for cancerous tissues in the breast and in the liver.

Simulated results for enhanced hyperthermia breast cancer were obtained using HFSS and SEMCAD X and values for the SAR and transient temperature in the healthy tissue and the tumor were presented. Using Penne's bioheat transfer equation and comparing results with and without iron oxide nanoparticles injected in the tumor, it was seen that the presence of nanoparticles allowed for the required increase in temperature in a short period of time. Various characteristics of the nanoparticles such as size, concentration, and susceptibility were considered. It was seen that a radius of 18 nm and a concentration of 40 mg/mL provided the most desirable results. Temperatures in the tumor reached that required to kill the cancer cells while the healthy tissue remained at a safe temperatures.

Experiments were conducted on a phantom model and the results validated those obtained through simulations.

As the blood flow in the body plays an important role in maintaining the body temperature, the effect of blood perfusion in magnetic fluid hyperthermia was also studied. Here, a tumor in the liver was injected with nanoparticles and five different blood perfusion rates were studied. Using a human male model, available in SEMCAD X, and appropriate values for the dielectric constant and conductivities in the tissue, the incremental increase in the temperature was obtained in the liver and in the tumor. When the blood perfusion rate in the tumor was low, as in the case found in liver tumors, the rise in temperature was higher in the tumor than in the healthy tissue.

Experiments were done using a liver phantom model and allowing 0.35% saline solution flow through it to simulate blood flow. The results obtained agree with those of the SEMCAD X simulation.

It was shown that the use of magnetic nanoparticles does provide a more effective hyperthermia treatment for cancerous tumors in the breast and liver.

# REFERENCES


[1] I.M Zaryabova and M. Ivanova , "Electromagnetic field occupational exposure: non-thermal vs. thermal effects," *Electromagn. Biol Med*., vol. 32, pp. 145-154, Jun. 2013.

[2] C. Johnson A. Guy, "Nonionizing Electromagnetic Wave Effects in Biological Materials and systems," *IEEE Biolog. Effe. of Electrom. Radiation*, pp. 47-73, 1983.

[3] A. Vorst et al., *RF Microwave Interaction with Biological Tissues*. Wiley Series in Microwave and Optical Engineering, Honoken NJ, 2006.

[4] H. P Schawn and G. Morri, "The Absorption of Electromagnetic Energy in Body Tissues," *IEEE Biolog. Effe. of Electrom. Radiation*, pp. 6-21, 1983.

[5] J.W. Hand and G. Ter Haar, "Heating techniques in hyperthermia," *Br. J. Radiol*., vol.54, pp. 443-466, 1981.

[6] I. Green, "Hyperthermia alone or combined with chemotherapy for treatment of cancer," *AHCPR Health Technology Reports*, vol. 2, pp.1-16, 1991.

[7] P. Wust et al., "Hyperthermia in combined treatment of cancer," *Lancet Oncol*., vol. 3, pp. 487-497, 2002.

[8] E.R Lee, "Electromagnetic superficial heating technology," *Thermoradiotherapy and thermochemotherapy*, Springer-Verlag, pp.193-217, 1995.

[9] S. Wust et al., "Electromagnetic deep heating technology," *Thermoradiotherapy and thermochemotherapy*, Springer-Verlag, pp.219-251, 1995.

[10] R. Antolini et al., "Absorbed power distributions from single or multiple waveguide applicators during microwaved hyperthermia," *Phys. Med. Biol*., vol. 31, pp. 1005-1019, 1986.

[11] K.S Cole and R.H Cole, "Dispersion and absorption in dielectrics I. Alternating current characteristics," *The J. of Chemical Physics*, vol. 9, pp. 341-351, 1941.

[12] C. Gabriel, "Compilation of the Dielectric Properties of Body Tissues at RF and Microwave Frequencies," King's College, London, Department of Physics, 1996.

[13] E.C Van E.Cet al., "Regional hyperthermia of pelvic tumours using the Utrecgt Coaxial TEM system: a feasibility study," *Int. J. Hyperthermia*, vol. 11, pp.173-186, 1995.

[14] Y. Kotsuka et al., "Development of inductive regional heating system for breast hyperthermia," *IEEE Trans. Microw. Theory Tech*., vol. 48, 1807-1814, 2000.

[15] B.Mortimer and S. L. Osborne, "Tissue heating by short wave diathermy," The Journal of the American Medical Association, vol. 103, pp. 1413‑1418, 1935.

[16] W. T. Szymanowski and R. A. Hicks, "Further studies of biologic action of ultra-high frequency currents," The Journal of Infectious Diseases, vol. 50, p. 471, 1932.

[17] R.K Gilchrist et al, "Selective Inductive Heating of Lymph," *Ann. of Surgery*, vol. 146, pp. 596-606, 1957.

[18] W. W. Shingleton, "Selective heating and cooling of tissue in cancer chemotherapy," Annals of Surgery, vol. 156, pp. 408‑416, 1962.

[19] M. von Ardenne and P. G. Reitnauer, "On the effect of hyperthermia on Ehrlich mouse ascites cancer cells," Archiv f¨ur Geschwulstforschung, vol. 26, no. 3, pp. 184‑185, 1965.

[20] M. von Ardenne, "Principles and 1977 concept of cancer multistep therapy. Physiological fundamentals of the new timing. Selectotherm local hyperthermy," Archiv f¨ur Geschwulstforschung, vol. 48, no. 6, pp. 504‑520, 1978.

[21] M. von Ardenne and W. Kr··uger, "Combined whole-body and local hyperthermia for cancer treatment: CMT selectotherm technique," Progress in Clinical and Biological Research, vol. 107, pp. 705‑713, 1982.

[22] H. S. Reinhold, J. van der Zee, N. S. Faithfull, G. van Rhoon, and J. Wike-Hooley, "Use of the Pomp-Siemens hyperthermia cabin," National Cancer Institute Monograph, vol. 61, pp. 371‑ 375, 1982.

[23] F.K. Storm et al., "Clinical RF hyperthermia by magnetic-loop induction: a new approach to human cancer therapy," *IEEE Trans. Microw. Theory Tech*., vol. 30, pp. 1124-1158, 1982.

[24] M. A. Astrahan et al., "Heating characteristics of a helical microwave applicator for transurethral hyperthermia of benign prostatic hyperplasia," Int. J. Hyperthermia 7, 141–155, 1991.

[25] C. Moran et al., "Size-dependent joule heating of gold nanoparticles using capacitively coupled radiofrequency fields," *Nano. Research*, vol.2, pp. 400-405, May 2009.

[26] R. Ben-Yosef, D. S. Kapp, "Direct clinical comparison of ultrasound and radiative electromagnetic hyperthermia applicators in the same tumours," International Journal of Hyperthermia , 11, 1-10, 1995.

[27] P. F. Turner, A. Tumeh, and T. Schaefermeyer, "BSD-2000 approach for deep local and regional hyperthermia: physics and technology," Strahlentherapie und Onkologie, vol. 165, no. 10, pp. 738‑741, 1989.

[28] P. F.Turner and T. Schaefermeyer, “BSD-2000 approach for deep local and regional hyperthermia: clinical utility,” Strahlentherapie und Onkologie, vol. 165, no. 10, pp. 700‑704, 1989.

[29] P. Wust, H. Fähling, T. Helzel et al., “Design and test of a new multi-amplifier system with phase and amplitude control,” International Journal of Hyperthermia, vol. 14, no. 5, pp. 459‑477, 1998.

[30] H. J. Feldmann, M. Molls, S. Kr··umplemann, M. Stuschke, and H. Sack, “Deep regional hyperthermia: comparison between the annular phased array and the sigma-60 applicator in the same patients,” International Journal of Radiation Oncology, Biology, Physics, vol. 26, no. 1, pp. 111‑116, 1993.

[31] Vogel TJ, Mack MG, Straub R et al. Percutaneous thermoablation of malignant liver tumors, Fortschr Rontgenstr 2000; 172:12-22.

[32] H.H. Pennes., "Analysis of tissue and arterial blood temperature in the resting forearm," *J Appl Physiol*, vol. 1, pp. 93-122, 1948.

[33] E.H. Liu et al., "Model analysis of tissue responses to transient and chronic heating," *Ann. Biomed Eng*, vol. 31, pp. 1007-1048, 2003.

[34] K.B Ocheltree and L.A Frizzell, "Determination of power deposition patterns for localized hyperthermia: a steady-state analysis," *Int. J. Hyperthermia*, vol. 3, pp. 269-279, 1987.

[35] K.B Ocheltree and L.A Frizzell, "Determination of power deposition patterns for localized hyperthermia: a transient analysis," *Int. J. Hyperthermia*, vol. 4, pp. 281-296, 1987.

[36] Guidelines for limiting EMF exposure, International Commission on Non-Ionizing Radiation Protection, Health Phys., vol. 66, pp. 508-512, 1998.

[37] IEEE Standards for Safety Levels Respects to Human Exposure to Radio Frequency Electromagnetic Fields, 3 KHz to 300 GHz , IEEE C95.1-1991, 1992.

[38] S. Santra et al., "Nanoparticles and their use for multifunctional bioimaging, " Google Patents, 2012.

[39] J.S Weinstein et al., "Superparamagnetic iron oxide nanoparticles: diagnostic magnetic resonance imaging and potential therapeutic applications in neurooncology and central nervous system inflammatory pathologies, a review," *J. Cereb. Blood Flow Metab*., vol. 30, pp. 15-35, Jan 2010.

[40] A. Babu et al., "Nanoparticle-Based Drug Delivery for Therapy of Lung Cancer: Progress and Challenges," *J. of Nanomaterials*, vol. 2013, pp. 1-11, 2013.

[41] P.P Vaishnava et al., "Magnetic relaxation and dissipative heating in ferrofluids," *J. of Appl. Physics*, vol. 102, pp. 1-5, 2007.

[42] F. Danhier et al., "To exploit the tumor microenvironment: passive and active tumor targeting of nanocarriers for anti-cancer drug delivery," *J. Control Release*, vol. 148, pp. 135-146, 2010.

[43] A. Jordan et al., "Inductive heating of ferrimagnetic particles and magnetic fluids: physical evaluation of their potential for hyperthermia," *Int. J. Hyperthermia*, vol. 9, pp. 51-68, 1993.

[44] L. Shang et al., "Engineered nanoparticles interacting with cells: size matters," *J. of Nanobiotechnology*, vol. 12, pp 5-15, 2014.

[45] R.E Rosensweig, "Heating magnetic fluid with alternating magnetic field," *J. Magn. Magnetic Materials*, vol. 252, pp. 370-374, 2002.

[46] B. Fischer Bet al., "Brownian relaxation of magnetic colloids," *J. of Magn. Magnetic* Materials, vol. 289, pp. 74-77, 2005.

[47] Semcad X., SIM4LIFE, SPEAG - Schmid & Partner Engineering AG, http://www.semcad.com.

[48] D.S Yoo, "The dielectric properties of cancerous tissues in a nude mouse xenograft model," Bioelectromagnetics, vol. 25, pp. 492-497, 2004.

[49] J. Smit and H. P. J. Wijn, Ferrites. New York: Wiley, 1959.

[50] Handbook of Microwave Ferrite Materials. New York: Academic, 1965.

[51] R. Hergt et al., "Physical limits of hyperthermia using magnetite fine particles," IEEE Trans. Magn., vol. 34, pp. 3745-3754, 1998.

[52] R. Ortega-Palacios et al., "Measurement of breast - tumor phantom dielectric properties for microwave breast cancer treatment evaluation," 2010 7th International Conference on Electrical Engineering Computing Science and Automatic Control (CCE), 2010.

[53] J. Volakis. Antenna Engineering Handbook, Fourth Edition, June 2007.

[54] P. Moroz P et al., "Tumor response to arterial embolization hyperthermia and direct injection hyperthermia in a rabbit liver tumor model," *J. Surg. Oncol*., vol. 80, pp. 149–156, July 2002.

[55] C.W Song et al., "Implication of blood flow in hyperthermic treatment of tumors," *IEEE Trans. Biomed. Eng*., vol. 31, pp. 9-16, Jan.1984.

[56] H.R Shibata and L.D MacLean, "Blood flow to tumors," *Prog. Clin. Cancer*, vol. 2, pp. 33–47, 1966.

[57] R.K. Jain and K. Ward-Hartley, "Tumor Blood Flow-Characterization, Modifications, and Role in Hyperthermia," *IEEE Trans.Sonics Ultrason.*, vol. 31, pp. 504-525, 1984.

[58] L. Shargel and A.B.C Yu, "Applied Biopharmaceutics and Pharmacokinetics", 2nd ed., Appleton- Century- Croft, Norwalk, CT, 1985.

[59] J.M Llovet et al., "Arterial embolisation or chemoembolisation versus symptomatic treatment in patients with unresectable hepatocellular carcinoma: a randomised controlled trial, " *Lancet*, vol. 359, pp. 1734-1739, 2002.